FACULDADE DE ENGENHARIA DA UNIVERSIDADE DO PORTO

Real-Time Passive Acoustic Tracking of Underwater Vehicles

José Francisco Ramos Valente

DISSERTATION THESIS

MASTER IN ELECTRICAL AND COMPUTERS ENGINEERING

Supervisor: Prof. Dr. José Carlos Santos Alves

Co-Supervisor: Prof. Dr. Nuno Alexandre Lopes Moreira da Cruz

July 26, 2016

Resumo

Com o crescente interesse na exploração oceânica, os sistemas robóticos marinhos estão a ganhar uma nova importância em diversos campos científicos e domínios industriais. Neste contexto, torna-se evidente que os Veículos Submarinos Autónomos (AUV - Autonomous Underwater Vehicles) são instrumentos relevantes para atividades de investigação no mar, devido à sua versatilidade para diferentes missões, combinados com custos baixos de fabrico, operação e manutenção, quando comparados com veículos submarinos tripulados.

AUVs de longo curso, como os planadores subaquáticos, são capazes de realizar missões de grande alcance com total autossuficiência energética. Durante essas missões de longo curso, esses veículos passam grande parte do tempo submersos, navegando sem conhecimento preciso da sua localização ou rota, podendo ser severamente afetados pelas correntes oceânicas. Quando estes veículos estão submersos deixam de receber as ondas eletromagnéticas emitidas por satélites e por isso os sistemas de localização e navegação baseados em sinais de rádio-frequência correntemente usados à superfície, como o GPS, tornam-se inúteis.

A localização de AUVs é feita geralmente por sistemas de posicionamento acústico subaquáticos. No entanto, o funcionamento destes sistemas está limitado ao alcance relativamente reduzido dos transmissores acústicos, e requerem o apoio de uma infraestrutura localizada numa posição geográfica conhecida. Por este motivo os sistemas tradicionais de localização acústica subaquática não são adequados para a localização de AUVs a uma escala oceânica. Uma solução já explorada em outros trabalhos consiste em usar um ou mais veículos de superfície para transpostar os sistemas necessários à localização de um AUV, devendo naturalmente ter uma capacidade de autonomia e um alcance de operação similar ao AUV.

O objetivo deste trabalho é o desenvolver um sistema de posicionamento subaquático de baixo custo e de baixo consumo energético, para ser usado a bordo de um veículo de superfície de longo curso. Pretende-se que este sistema permita estimar a posição de um AUV, possibilitando ao veículo de superfície acompanhar o AUV durante as missões de longo curso enquanto está submerso.

O sistema de localização acústica passiva desenvolvido neste trabalho tem uma topologia idêntica à do *ultra-short baseline*, operando em tempo real. São usados apenas dois hidrofones para calcula a posição a duas dimensões de uma fonte acústica submersa emitindo um sinal conhecido, com base na integração de medições da direção do som ao longo do tempo. A direção de chegada da onda sonora é estimada pela diferença de tempo de chegada (TDOA) entre os dois sinais adquiridos pelos hidrofones, colocados próximos um do outro para atenuar a disparidade do canal acústico. Neste trabalho é proposto um método alternativo para o cálculo do TDOA, que consiste na determinação do início dos sinais recebidos recorrendo à deteção de uma série de transições por zero que são semelhantes em cada um dos sinais recebidos.

Este processo foi implementado num dispositivo Zynq da XILINX, combinando um sistema de processamento digital dedicado na parte lógica programável com uma aplicação de software

executada no processador ARM embarcado. Como fonte acústica subaquática foi usado um transmissor comercial de 35 kHz, sendo os sinais adquiridos pelos dois hidrofones processados com uma frequência de amostragem de 2 Msps. Os resultados obtidos em ensaios de campo realizados numa marina permitiram obter a posição do transmissor acústico com um erro inferior a 1.5 m.

Abstract

With the growing interest in oceanic exploration, marine robotic systems are gaining a new importance in diverse scientific fields and industrial domains. In this context, it is clear that Autonomous Underwater Vehicles (AUV) are relevant instruments for research activities in the sea because of their adaptability for different missions, combined with a low-cost deployment and maintenance in comparison with manned vehicles.

Long endurance AUVs, like the underwater gliders, are capable of performing very long range missions with complete energy self-sufficiency. During such long-term missions, these vessels usually spend most of their time submerged, navigating without a precise knowledge of their actual location and course, that may be severely affected by ocean currents. When these vehicles are submerged, they fail to receive the electromagnetic waves emitted by satellites. Therefore the localization and navigation systems based on radio frequency signals, like the GPS currently used above the surface become useless.

The localization of AUVs is usually done by underwater acoustic positioning systems. However, the operation of these systems is constrained by the limited range of the acoustic transmitters, and require the support of an infrastructure located at a known geographic positioning. Because of this, the traditional underwater acoustic localization systems are not suitable for the localization of AUVs at the oceanic scale. One solution already exploited by other works uses one or more surface vehicles to carry the acoustic support infrastructure, which must have an autonomy and range of operation similar to the AUV being located.

The goal of this work is to develop a low-cost and low-power underwater positioning system to be used on board of a single long-endurance surface vehicle. This system estimates the AUV position and allows the surface vehicle to accompany the AUV during long-range missions while submerged.

The passive acoustic localization system developed in this work has a topology identical to the ultra-short baseline and is capable of operating in real-time. Only two hydrophones are used to determine the two-dimension position of a known underwater acoustic source, based on the integration along time of the direction of the received sound wave. The direction of arrival of the sound wave is calculated by the time difference of arrival (TDOA) between the signals acquired by the hydrophones, closely placed to attenuate the disparity of the acoustic channel. We propose an alternative method to calculate the TDOA, consisting in the detection of the beginning of the signals by discovering a series of zero crossing samples looking alike in each received signal and then calculating the time difference between them.

This process was successfully implemented in a XILINX Zynq device, combining a custom designed digital signal processing system implemented in the programmable logic (PL) part, and a software application running in the embedded ARM processor. A commercial 35 kHz underwater acoustic beacon was used as the transmitter and the signals acquired by the hydrophones were processed at a 2 Msps sampling rate. The results obtained in field trials conducted in a marina allowed to determine the position of the acoustic beacon within an error of less than 1.5 m.

Agradecimentos

Em primeiro lugar, agradeço ao Professor José Carlos Alves, velejador, orientador e amigo, por todo o apoio não só na dissertação mas ao longo destes 5 anos, por todos os projetos, viagens, horas despendidas e piadas incompreendidas.
Aos meus pais que sempre acreditaram em mim e que me apoiaram em todos os esquemas, planos e projetos desde pequeno.
À Maria pela incansável revisão, assistência na piscina e no mar, apoio e paciência para me aturar, sem nunca deixar de gostar.
Ao Perestrelo pelos incontáveis finos e atrasos que tornam Munique inesquecível.
Ao Miguel por todos os trabalhos, relatórios e projetos nestes 5 anos e não só.
A todos os colegas que passaram a amigos nos inúmeros jantares e noites sem dormir.

José Francisco Valente

"The pessimist complains about the wind
The optimist expects it to change
The realist adjusts the sails"

William Arthur Ward

Contents

List of Figures

List of Tables

List of Abbreviations

ADC	Analog to Digital Converter
ASV	Autonomous Surface Vehicles
AUV	Autonomous Underwater Vehicles
DAC	Digital to Analog Converter
DMA	Direct Memory Access
DOA	Direction of Arrival
DSP	Digital Signal Processing
FASt	FEUP Autonomous Sailboat
FIR	Finite Impulse Response
FPGA	Field-Programmable Gate Array
GCC	General Cross-Correlation
GIB	GPS Intelligent Buoys
I2C	Inter-Integrated Circuit
INS	Inertial Navigation System
LBL	Long Baseline
MLBL	Moving Long Baseline
PID	Proportional Integral Derivative
PL	Programmable Logic
ROV	Remotely Operated underwater Vehicles
RSSI	Received Signal Strength Indicator
SBL	Short Baseline
SLAM	Simultaneous Localization and Mapping
SoC	System on Chip
TDOA	Time Difference of Arrival
TOA	Time of Arrival
TOF	Time of Flight
USBL	Ultra Short Baseline

Chapter 1

Introduction

On Earth the oceans cover almost 71% of its total surface, being of paramount importance for the human life in the whole planet as they influence the global climate and weather patterns. Oceans are a vast habitat for more than 230,000 known species, although much of the oceans depths still remain unexplored, hiding valuable resources in the water, on the seafloor and also beneath it.

With this in mind, it is comprehensible the growing interest in oceanic exploration. Marine robotic systems are gaining a new importance in diverse scientific fields such as biology, oceanography, and meteorology. Also, in industrial domains as in offshore oil and gas exploration, seafloor mining, and in the areas of surveillance and security of marine borders and seaborne facilities. In this context, it is clear that Autonomous Underwater Vehicles (AUV) or Remotely Operated underwater Vehicles (ROVs) are relevant instruments for research activities in the sea because of their adaptability for different missions, combined with the low-cost deployment and maintenance in comparison to manned vehicles.

Long endurance AUVs, such as the underwater gliders, are capable of performing very long range missions with complete energy self-sufficiency. During such long-term missions, these vessels usually spend most of their time submerged, navigating along a straight course controlled by an electronic compass or inertial navigation system, but without knowing their actual location and path that may be severely affected by ocean currents or waves. Nowadays, these vehicles are the only autonomous underwater platforms capable of collecting ocean data for several months without requiring any local assistance. Therefore, they are a powerful tool to improve the knowledge of the oceans. According to the records provided by the Everyone's Gliding Observatories organization, since 2004 more than 350 gliders have been deployed in the oceans and presently (end of June 2016) 7 gliders are reported as being active.

When these vehicles are on a mission, it is highly desirable to know their current location. While at the sea surface the global navigation satellite systems, such as the GPS, are able to provide real-time positioning with incredible accuracy. However, when these vehicles submerge, they fail to receive the electromagnetic waves emitted by satellites, and therefore these radio frequency-based navigation systems become useless.

In addition to the inability to use satellite positioning, data communication underwater also

suffers from the strong attenuation of electromagnetic waves in water. Because of this, the most robust way to communicate underwater is by using acoustic signals, although with very low bandwidths and ranges. Additionally, for an AUV engaged in a long-term oceanic mission, the communication of data to a shore base station can only be effectively done while at the surface using satellite communications, or relying on an acoustic communication link to a surface vehicle in range to act as a relay for satellite data networks.

The localization of AUVs is usually done by underwater acoustic positioning systems. These systems consist of using acoustic transmitters and receivers to determine the relative position of the underwater vehicles, based on measurements of distance by the propagation time of acoustic signals. However, the operation of these systems is constrained in practice by the limited range of the acoustic transmitters, and because they require the support of an infrastructure located at a known geographic position, they are not suitable for the localization of AUVs at the oceanic scale.

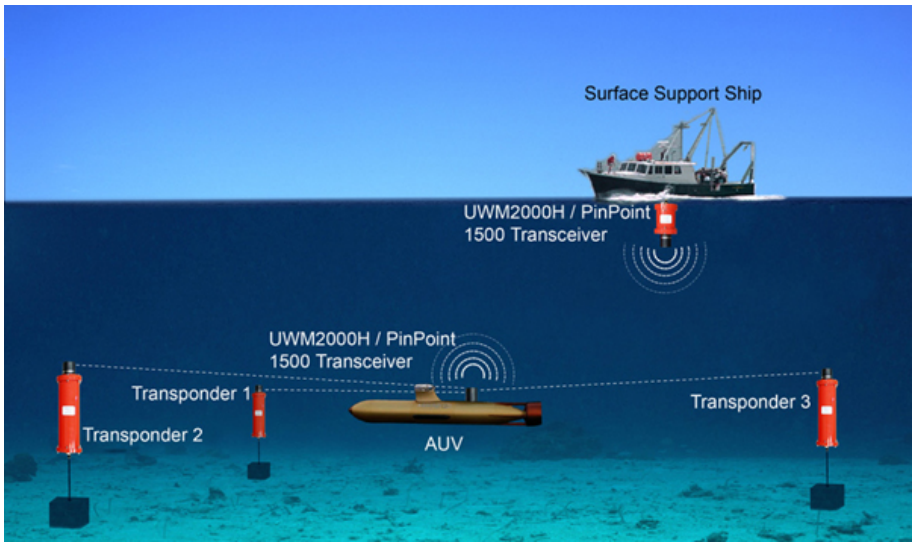

Figure 1.1: Underwater acoustic positioning system, LinkQuest Inc.

These positioning systems are already available in the market, supplied by several companies such as the LINKQUEST INC., which has several products for this purpose. Figure 1.1 represents a simplified diagram of an underwater acoustic positioning system, which shows a surface vehicle as the control station and three submerged transducers that are used to locate an AUV.

One solution for locating AUVs during long-range missions is to attach an underwater acoustic positioning system to one or more surface vehicles capable of similar long-range operation. To be effective, the surface vehicles must be able to accompany the AUV and stay in the range of the acoustic positioning system. Besides providing a localization infrastructure, the surface vehicles may also be used as relays to satellite data networks, thus offering a permanent communication link with the submerged vehicle, at the oceanic scale. (Papadopoulos et al., 2010)

1.1 Objectives

The goal of this work is to develop a low-cost and low-power underwater positioning system to be used on board of a single long-endurance surface vehicle, to estimate the AUV position and allow the surface vehicle to accompany the AUV mission while submerged. More important than determining an accurate position of the AUV, it is desirable to estimate an approximate location within a range of a few meters with low computational effort, and consequently requiring little energy for the computing tasks. Even with a rough localization data from the surface vehicle, it would be possible to make use of underwater acoustic communications to transmit data to the surface vehicle and then to a satellite network. The surface vehicle must be able to navigate faster than the AUV and with the same degree of autonomy and range of operation, what is necessary for establishing convenient navigation patterns to improve the estimation of the actual position of the AUV. With the continuous knowledge of the location of the submerged AUV, even if inaccurate, the surface vehicle can position itself to take advantage of favorable conditions for establishing acoustic communications and retrieve data from the AUV to relay to satellite data networks. For example, it is known that the acoustic communication along a vertical channel is less prone to several effects that affect the propagation of acoustic waves in the water, like multipath, reflections, and refractions at the transitions between water layers with different physical characteristics (temperature, salinity).

Autonomous sailing boats, Alves and Cruz (2008), fulfill the requirements of autonomy, range and speed for the application scenario envisaged above. Although the navigation performance of a sailing boat is highly dependent on the relative wind direction and speed, their utilization in such application will require the establishment of convenient sailing patterns around the estimated location of the (moving) AUV, to improve the accuracy of localization of the AUV while staying within the range of acoustic communications.

1.2 Project Overview

Long endurance autonomous underwater vehicles (AUV), such as electric underwater gliders capable of undertaking multi-month unassisted missions, suffer from the lack of real-time communications with the outside world, while submerged in remote ocean locations. In long range applications, it may be desirable to have real-time communications for retrieving data or remotely changing the mission parameters. As acoustic communications are the only practical mean to transmit data underwater, this problem can be mitigated by using a cooperative autonomous surface vehicle (ASV) capable of following at the surface the path of the submerged AUV and provide a relay to satellite data networks (Papadopoulos et al., 2010).

An underwater acoustic positioning system capable of being applied to an autonomous surface vehicle is the Ultra Short Baseline (USBL) referred in 2.3.3. The USBL is a half-duplex communication system, which requires having a receiver and transmitter at both ends, with negative impact in the complexity of the acoustic systems in the two vehicles. Besides, in long endurance vehicles

the power consumption (related directly to the demand of computation) is a critical factor that naturally affects the vehicle's autonomy.

This may be eased by attaching to the AUV a device transmitting a known acoustic signal and calculating the direction of the sound wave relative to an array of hydrophones, by measuring the time difference of arrival (TDOA) of the sound wave to the different hydrophones. Employing an array of hydrophones in a moving surface vehicle makes it possible to determine a set of relative directions between the two moving vehicles. By adopting convenient routes by the surface vehicle, and assuming a higher velocity than the AUV, it is possible to combine those directions to extrapolate the relative position of the submerged device.

The tracking of the AUV can be relaxed because of the scale of the missions. A precision of a few meters in an oceanic scale is insignificant and is more important that the surface vehicle does not lose the link to the submerged vessel, granting a communication relay to the outside world.

1.3 Approach

The approach suggested in this work is to develop a system based on the USBL scheme but only with a transmitter in the AUV and a receiver in the surface vehicle, reducing the complexity of the system and the power consumption. This system has to be capable of measuring the direction of arrival of the underwater acoustic transmission, then, the surface vehicle has to accumulate the different directions along time and estimate the relative position of the underwater vehicle. This system does not need any type of synchronization or event trigger communication, just acting as a passive receiver that calculates the relative position of the AUV.

Contrary to the conventional USBL system, it is not possible to obtain a range for each single transmission. However, as explained above, exploiting a higher velocity of the surface vehicle it will be possible to determine an approximate location by combining several directions obtained from known positions of the surface vehicle.

In order to make the system more flexible and not requiring the installation of specific equipment in the AUV, we decided to use commercially available underwater acoustic beacons as the acoustic transmitter. These beacons have their own power supply, and so they do not need to be electrically connected to the AUV power or computing system; the transmitter simply needs to be mechanically attached to the AUV body.

The surface vehicle needs to have two or more hydrophones to successfully estimate the direction of arrival (DOA) of an acoustic signal emitted by the AUV. The time difference of arrival (TDOA) is computed with the phase-shift between pairs of signals recorded by distinct hydrophones. Then using the multilateration technique referred in section 2.5 and the spatial distribution of the hydrophones, it becomes possible to calculate the relative angle of arrival. In this work, it was decided to employ only two hydrophones for the prototype system because with a proper alignment of the hydrophones it is sufficient to determine the direction of the received sound wave in two dimensions, thus reducing the complexity of the hardware structure. However,

the system developed can be easily extended to three or even more hydrophones to improve the accuracy of the direction of arrival and of the estimated position.

1.4 Contributions

A major contribution of this thesis was the development of an alternative method to determine the time difference of arrival and its implementation in an embedded programmable system on chip (SoC). This method can easily be scaled to work with more hydrophones and ported to different re-configurable digital devices.

A paper was presented in the XII Jornadas Sobre Sistemas Reconfiguráveis - REC2016, University of Trás-os-Montes and Alto Douro (UTAD), on the 21st of June, 2016.

Finally, an abstract was submitted to review in the OCEANS'16 Monterey Student Poster Competition and was accepted to be included in the regular technical program. The conference will be held from 19th to 23rd of September, 2016.

1.5 Document Structure

Besides this introduction, the rest of the document is organized in more 5 chapters. Chapter 2, the state of the art, it is presented some of the work that is known for underwater acoustics and localization systems. We then proceed in chapter 3 to describe different approaches to determine the position of an underwater vehicle, developing a distinct method for this purpose.

The implementation in chapter 4, describes all the electronic systems used in this work, the digital implementation of the algorithm, and the software processing.

In chapter 5 is presented the initial laboratory experiments and conclusions. The analysis of the results obtained and presents all the configurations for the hardware implementation. Also describes and presents the results for the tracking of an underwater beacon in the field scenario.

Finally, we conclude by summarizing the results of this work and future work to be done.

Chapter 2

State of the Art

This chapter explores the techniques for localization of underwater vehicles used nowadays, describing different vehicles, methods, and topologies to achieve underwater localization. The principal focus of this work is on underwater acoustic localization systems for vehicles and devices operating in various underwater environments.

2.1 Underwater Vehicles

Since the first successful submarine built in 1620, the construction of underwater vehicles never stopped increasing. In this section, three leading technologies are considered.

1. **Manned Submersibles**
2. **Remotely Operated Vehicles (ROVs)**
3. **Autonomous Underwater Vehicles (AUVs)**

With so many different applications like scientific, commercial, and military missions, the manned submersibles, started to be too expensive to meet all these different requirements. Therefore, it appeared a new type of vehicles: the unmanned ROV (Remote Operated Vehicle). Because they are remotely operated from a surface support vessel, they are much cheaper to operate, easier to deploy and can reach virtually any depth in the Earth's oceans. Then, the next logic step was to make them autonomous, creating the AUVs, that are the most cost-effective alternative and versatile vehicles.

Autonomous underwater vehicles (AUVs) are versatile robotic submarines that are revolutionizing the way in which researchers and industry obtain marine data. Advances in technology have resulted in competent vehicles that have made possible new discoveries in the oceans and have dramatically reduced the cost of industrial and scientific surveying of the seabed. These vehicles range in size from man-portable lightweight AUVs to large diameter vehicles of over 10 meters length. Large vehicles have advantages in terms of endurance and sensor payload capacity; the smaller vehicles benefit significantly from lower logistics and cost.

The underwater glider is a type of AUV, that uses small changes in its buoyancy, combined with adjustable wings that convert vertical motion to horizontal, thereby propelling itself forward with very low power consumption. While not as fast as conventional AUVs, gliders using buoyancy-based propulsion represent a significant decrease in energy consumption, consequently increases the range and duration compared to vehicles propelled by electric motor-driven propellers, extending ocean sampling missions from hours to weeks or months, and the range to thousands of kilometers. This vehicles are so appealing to the community that a considerable number of companies start to produce them. Figure 2.1 shows one of the most successful commercial electric gliders in the market.

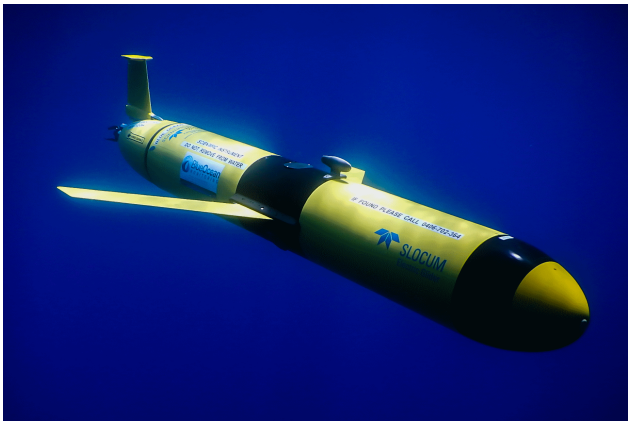

Figure 2.1: Slocum electric glider (Teledyne Webb Research Corporation, 2016).

2.2 Localization Techniques

The underwater vehicles have to navigate accurately in their missions, so, they need to know their position for the data gathering being of value.

Two different perspectives are possible: the AUV can determine its position relative to the infrastructure, but the system does not know where the vehicle is. Or the symmetric, the vehicle does not know its location, but the infrastructure is tracking its relative position.

In the next subsections, the focus will be in the three most used methods to get the actual position and to navigate in underwater conditions.

2.2.1 Inertial Navigation Systems and Dead Reckoning

An inertial navigation system (INS), can calculate the position of a vehicle using accelerometers and gyroscopes. By integrating the accelerations twice in time and adding the rotational speed they can estimate the position based on the previous estimates. Position drift rates, for high-quality commercial grade INS units are on the order of few kilometers per day (Safran Electronics Defense, 2014), but, the cost, power consumption, and size have historically made INS systems unattractive for small AUVs.

Dead reckoning is another technique used to positioning AUVs, by integrating the vehicle velocity along time to obtain new position estimates. This is accomplished by determining the relative velocity components with water speed sensors, and combining with the orientation of the vehicle measured by a compass. One of the problems with this technique is the presence of an ocean current that will add a velocity component with respect to ground, which is not measured by water speed sensors. Therefore, dead reckoning for power-limited AUVs, operating at small speeds (3-6 knots), involving water-relative speed measurements can generate extremely weak position estimates (Leonard et al., 1998).

2.2.2 Geophysical Positioning

Geophysical positioning refers to any method that utilizes external environmental features for localization. Basically, by gathering information about the surrounding terrain and matching that information to an onboard map or database of terrain information. When the vehicle has a match to the database, then it knows its location on the map. These techniques take advantage of simultaneous localization and mapping (SLAM) algorithms for refining their position. The most popular categories are the following:

- **Optical**

  Based on the use of cameras to capture images of the surrounding, and then, matching these images to navigate. Disadvantages for optical systems in underwater environments include the reduced range of cameras, due to the water turbidity, susceptibility to scattering and inadequacy of lighting. In addition, visual odometry and feature extraction rely on the existence of static features in range of the vision systems, what only happens when navigating close to the sea floor. Therefore, optical underwater navigation methods are particularly well suited to a small-scale mapping of environments rich in static features.. Examples include ship hulls or shipwreck inspections (Paull et al., 2014).

- **Sonar**

  Utilized to detect acoustically features in the environment that could be used as navigation landmarks. With bathymetric sonar, features can be extracted almost directly from the scans. With side-scan (imaging) sonar, feature extraction is achieved through processing of imagery (Paull et al., 2014). Like the optical systems, after the collection of the surrounding features, it can be matched with known specific marks.

2.2.3 Acoustic Localization

Acoustic energy propagates appreciable distances in the ocean, in comparison with electromagnetic energy. For this reason, it is highly used for underwater localization and communication systems.

Underwater Acoustic Channel

The underwater acoustic channels have specific propagation features and are mainly characterized by the following (Tan et al., 2011):

- **Long propagation delay**

  The speed of sound on fresh water, at a temperature of 25 °C, is 1482 $\mathrm{m\,s^{-1}}$, which is approximately 4.5× the speed of sound in the air and five orders of magnitude of the speed of radio waves in the air. This has a direct impact on the available bandwidth, the latency of communications and even a slow vehicle may induce significant Doppler shift. Therefore, the errors due may become significant.

- **Multipath propagation**

  Multipath is the propagation phenomenon that results in signals reaching the receptor by two or more paths. Causes of multipath in the ocean include differences in the water temperature, pressure, and salinity, provoking the refraction of the signal. Also, multipath interference includes destructive interference and phase shifting of the signal. As a result, multipath causes indirect signals that can be mistaken for the direct signal and may significantly impact the accuracy of distance and phase estimations.

- **Sound speed variation**

  As mentioned in the previous topic, the parameters of the water can change the properties of the sound propagation. With uncertainty in the sound speed, the accuracy of distance measurement based on the delay of the signal propagation may be degraded. In figure 2.2, shows how sound speed varies as a function of water depth.

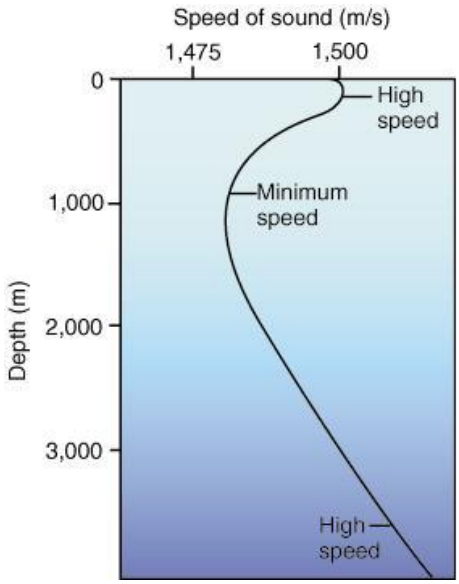

Figure 2.2: Sound speed variation due to water depth.

Range Measurement

In underwater acoustic localization, the distance can be measured by the following strategies, as explained in Tan et al. (2011):

- **Received Signal Strength Indicator (RSSI)**

  By measuring the received signal strength and comparing it with a range dependent signal attenuation model, it is possible to estimate the distance to the transmitter. However, it is difficult to achieve accurate ranging when multipath and shadow fading effects exist, as explained before. Since the path loss in underwater acoustic channels is usually time-varying and multipath effect can result in significant energy fading, the RSSI method is not a primary choice for underwater range measurement.

- **Time of Flight (ToF)**

  Based on the time difference of transmission and the reception of signals, the ToF, requires a transponder that on the arrival of transmitted signal replies with another signal. Then, when the transmitter receives the response it can estimate the distance between them, based on the knowledge of the sound speed . As discussed, the speed of sound can have deviations that cause errors in that measure.

- **Time of Arrival (ToA)**

  The Time of Arrival (ToA) method performs ranging based on the arrival time of the transmission, this presupposes that the receiver knows the time that the transmission began, so, is needed some type of synchronization between them.

Knowing the various distances to different references or with distinct distances in time, a system based on range measurement can use trilateration to calculate the relative position between them, as in a similar way used in current Global Navigation Satellite Systems. Another technique that can determine the relative position is by combining the distance and the direction of arrival (DOA) of the signal.

2.3 Underwater Acoustic Positioning Systems

Underwater acoustic positioning systems are commonly used in a wide variety of underwater applications, including oil and gas exploration, salvage operations, marine sciences and archaeology, security and military operations. They are used for tracking and as a tool for divers and underwater vehicles to navigate safely. These systems use the Time of Flight to measure the distances and also can use the phase shifting for measuring the direction of the diver or asset being tracked from a set of reference points, referred to as baseline stations. With the distance between the baseline stations taking into account, these systems are broadly categorized into Long Baseline (LBL), Short Baseline (SBL) and Ultra Short Baseline (USBL) (Tan et al., 2011).

2.3.1 Long Baseline (LBL)

The name derives from the fact that the distance between the baseline stations is long, typically ranges from 50 m to more than 2000 m (Rowan, 2008). In this system, a set of three or more baseline transponders is deployed on the sea floor along the edge of the area of operation. Typically, is used the Time of Flight technique, that requires an interrogation signal from the transponder and receiving a reply from the target. The signal propagation times are then used to compute the distances between them. Combining this information with the depth data from pressure sensors it is possible to calculate the position using trilateration. This location is relative to the baseline transponders but if the geographic position of the baseline transponders is known, it is easy to convert into geo-referenced coordinates. In figure 2.3, the four sub-sea transponders are localizing the surface platform and the two vehicles.

The topology can be inverted too, where the baseline transponders are applied to the surface, like in a moving platform, a ship or buoys. LBL systems provide high accuracy, better than 1 m. Manufacturers of LBL systems include Applied Acoustics (Transponders for LBL systems), Desert Star Systems LLC (AquaMap LBL systems), LinkQuest Inc. (Pinpoint LBL System), Nautronix (NASNet LBL system), Sonardyne (Fusion LBL system), Kongsberg Maritime and Sonatech (seafloor transponders).

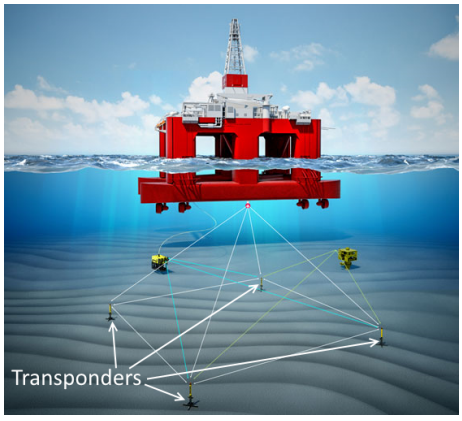

Figure 2.3: Long Baseline, LBL system (Kongsberg Maritime).

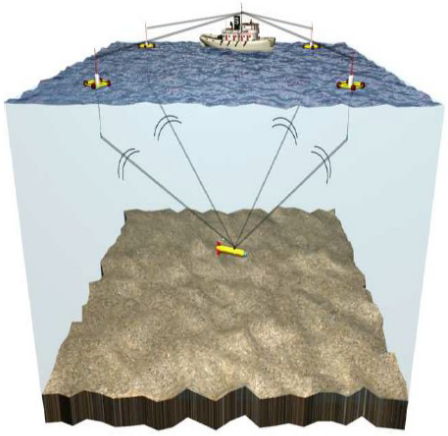

Figure 2.4: GPS Intelligent Buoys (GIB) (Alcocer et al., 2006).

The GPS Intelligent Buoys, GIB as explained in Alcocer et al. (2006), can be viewed as inverted LBL system. Instead of deploying the baseline transponders on the seafloor, they are installed on GPS equipped buoys that are either drifting or moored (Thomas, 1998). In a typical scenario, several GIBs are deployed over a given area of operation where the total number required is determined by the size of the operation area and the desired accuracy (precision of centimeters to a meter level in real time is achievable). In figure 2.4 the four buoys at the surface are tracking the underwater vehicle. GIB uses the one-way acoustic signal transmission from the emitter to buoys as compared to the round-trip transmission of LBL, SBL, and USBL making it less susceptible to reflections from the surface or other undersea structures. The GIB system is patented technology

that has been developed by ORCA Instrumentation and French R&D firm Advanced Concept and System Architecture.

2.3.2 Short Baseline (SBL)

SBL systems are characterized by the distance of the transducers that varies between a few tens of meters, with these distances, is possible to implement the systems on floating platforms, like boats, ships or barges. As in LBL systems, the ToF technique is used to measure the signal propagation time of acoustic signals between transponders and target to compute the distance and then trilateration to determine the position, often with supplementary depth data from a pressure sensor. The accuracy of SBL improves as the distance between baseline transponders increases and can achieve similar performance levels as seafloor mounted LBL systems. When is used on smaller vessels that reduce the distance between transponder, the accuracy is deteriorated. SBL systems are popular with research groups and have been employed in Antarctica expeditions to track vehicles operating under the ice, e.g. Project SCINI (scini.mlml.calstate.edu). In figure 1.1, the ROV (B in the figure), is being tracked by the three traducers placed on the surface vehicle.

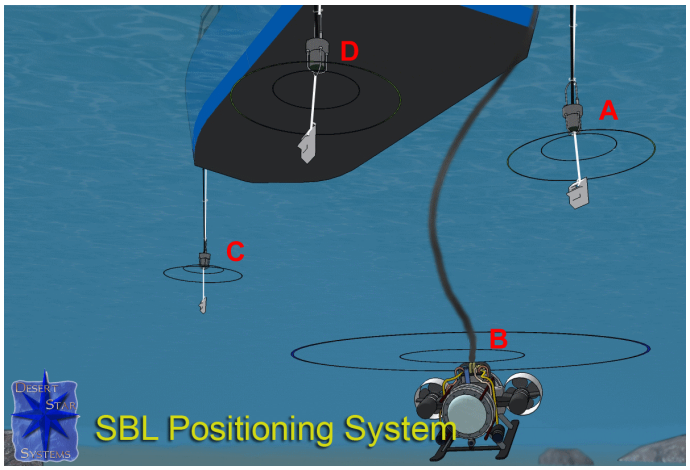

Figure 2.5: Short Baseline, SBL system (Desert Star Systems, 2015).

2.3.3 Ultra Short Baseline (USBL)

USBL is an evolution of the SBL, instead of few tens of meters apart, the transducers are separated by typically less than 10 cm apart. This system is by far the most popular category of underwater positioning systems due to its easy deployment and fewer components. The transceiver sends an acoustic pulse, and when the transponder (mounted on the tracked object) detects it, it replies with its own acoustic signal. The Time of Flight of both the initial acoustic pulse and the response pulse are used to compute the distance between them. For measuring the direction of the signal received, it is used the phase shifting of the signals to calculate the direction of arrival (DOA) method, explained in section 2.5. The position is then obtained combining the distance and the angle from the transceiver to the transponder. This system is a more susceptible to the underwater propagation

problems in underwater acoustic channels, being less accurate in terms of positioning. Manufacturers of USBL systems include Nautronix, Sonardyne, IXSEA (GAPS pre-calibrated Ultra-Short BaseLine), Applied Acoustics (EASYTRAK USBL), LinkQuest (TrackLink USBL), Tritech (Micron Nav), EdgeTech (BATS), Kongsberg (HiPAP - High Precision Acoustic Positioning), and EvoLogics (USBL Acoustic Modem).

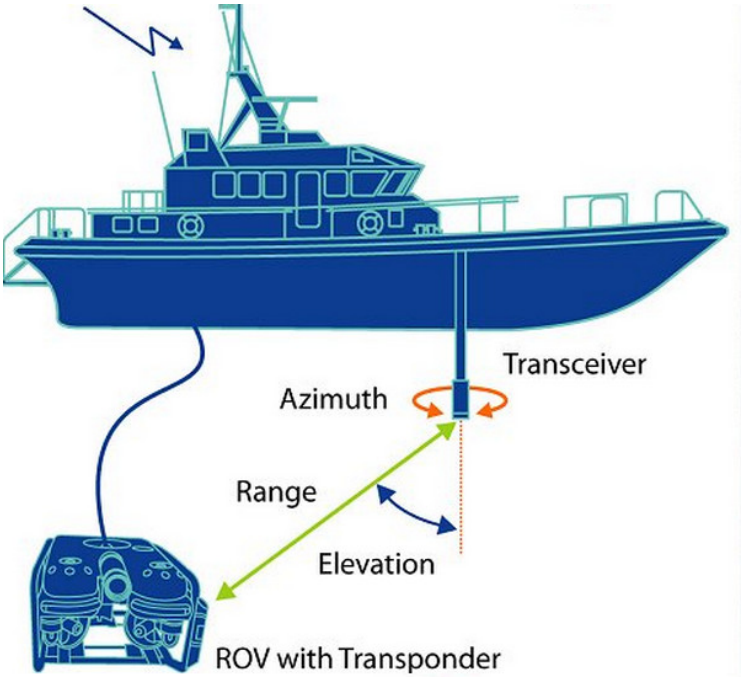

Figure 2.6: The USBL positioning method, Sonardyne International Ltd.

2.4 Time Difference of Arrival

The time difference of arrival (TDOA) method has been extensively used for passive acoustic source positioning by measuring the time difference between signals arriving in two or more hydrophones and then extrapolating the relative position of the acoustic source.

One of the methods used for estimating the time difference of arrival (TDOA) is the generalized cross-correlation (GCC) (Chen et al., 2006; Liu et al., 2012). The process consists in detecting the peak position of the correlation function between the two received signals, as the delay or time shift between them. Although being computationally intensive, this method is widely used because it can weaken the impact of the ambient noise on the accuracy of the signal lag estimation.

2.5 Direction of Arrival

The direction of arrival (DOA) is commonly estimated by measuring the TDOA and then applying one of the following methods.

- **Multilateration**

  The multilateration technique is based on hyperbolic positioning, one of the most common approaches for passive source localization, uses the time delays between pairs of sensors to characterize a curve of a constant time difference, which is a hyperbola (Dalskov and Olesen, 2014). Considering that the source distance is great compared to the sensor spacing, is acceptable to acknowledge the wave as a plane to the sensors. Therefore, the direction of propagation can be described by the asymptote of the hyperbola, and the slope of the asymptote will then define the direction relative to the axis of the sensors.

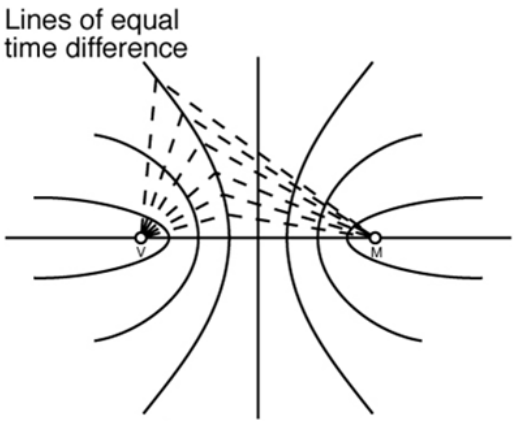

Figure 2.7: Diagram illustrating multilateration.

- **Trilateration**

  Trilateration is the process of determining relative positions of points by measuring distances, using spheres or circles (Schau and Robinson, 1987; Klungmontri et al., 2015). Considering only two sensors and that the source distance is great compared to the sensor spacing, the direction of arrival can be calculated by determining the angle of the intersection of two circles.

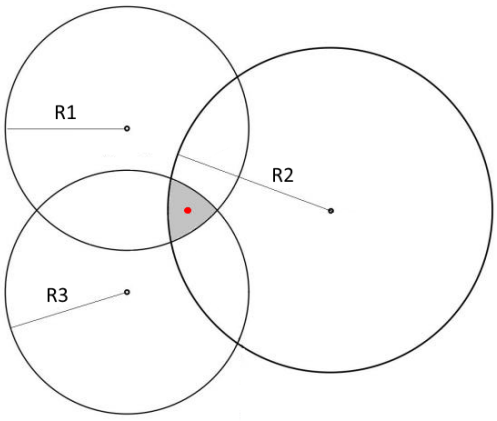

Figure 2.8: Trilateration in two dimensions.

2.6 Cooperative Localization

In cooperative localization, multiple vehicles can collaborate and help each other to navigate. To achieve this cooperation between different autonomous vehicles they have to communicate with each other to share data and determine or improve their position estimate (Rui and Chitre, 2010). This concept can be implemented in various manners, described below.

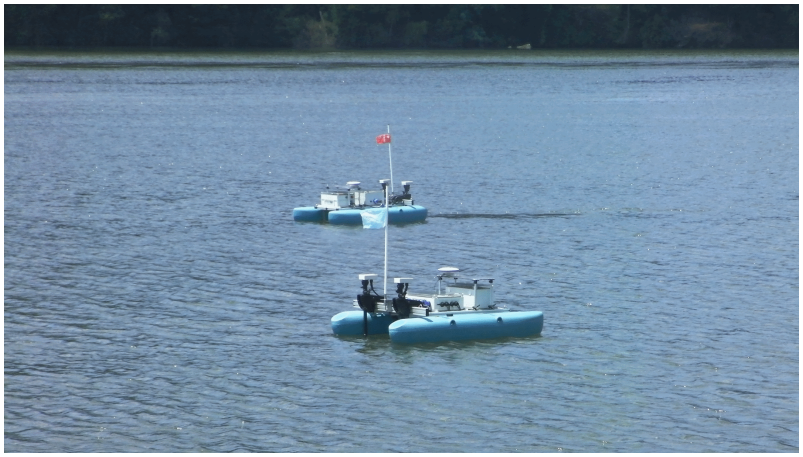

Figure 2.9: Autonomous Surface Vehicles cooperating to localize acoustic pinger in Ferreira et al. (2012).

The Moving Long Baseline (MLBL), is an inverted LBL system like GIB, but the buoys at the surface are replaced with Autonomous Surface Vehicles (ASVs) (Curcio et al., 2005; Folk et al., 2010). The surface vehicles have to know their position and transmit it to the AUV, and then it can use different estimation algorithms like the Extended Kalman Filter, Particle Filtering, or nonlinear Least Squares (Eustic et al., 2007) to estimate their own position.

The work reported in Papadopoulos et al. (2010) implements a different approach by having just a single maneuvering autonomous surface vehicle (ASV) to aid the navigation of an AUV. Applying the same principle as before, the surface vehicle shares their position with an underwater vehicle, then, the submerged vessel by using acoustic range measurements combined with the shared position can determine their own position.

Another approach in cooperative localization is a system that can track the underwater vehicle, but not share the position with it. Instead of the AUV having a transducer to communicate with the surface, it can have a simple beacon that will only transmit a signal repeated in time. Then, the surface vehicles can estimate the position of the AUV by acquiring the signal of the transmitter. In Ferreira et al. (2012) this topology is implemented with two ASVs tracking an autonomous underwater vehicle.

The work developed in this thesis intends to build a cooperative system for the localization of a submerged beacon, but using only one surface vehicle equipped with a passive acoustic direction finder based on the USBL topology. Instead of implementing a moving baseline created by the

two autonomous boats, a synthetic baseline is formed by measuring the angle of arrival in different locations. The ASV can establish known navigation paths by exploiting its higher velocity and maneuverability in comparison to the AUV. Therefore, tracking the underwater vehicle in real-time by accumulating several position estimates.

Chapter 3

Algorithm

As described in section 1.3, in this work we exploit the time difference of arrival between the signals acquired by two hydrophones, to measure the phase shift between them and determine the direction of arrival of the sound wave. An estimation of the position of the submerged sound source (attached to an AUV) can then be built by combining these directions with the relative movement between a (fast) ASV and a (slow) AUV. The experimental acoustic data acquired for the experiments carried out in this work were obtained using a custom acquisition and processing platform described in section 4.1. The preliminary laboratory experiments were done in a test tank of fresh water, with 4.75 m by 4.4 m and 1.7 m of depth. The field tests in a more realistic environment were performed in a marina and in the sea. The acoustic transmitter we used was a commercial underwater acoustic beacon transmitting a known sequence of short pulses of a 35 kHz signal (section 4.1).

One of the advantages of using passive tracking is to avoid the need for synchronization between the transmitter and the receiver. Therefore, the acoustic transmitter is not limited to any specific time slot to communicate. One objective of the system developed was to be easily adapted to other acoustic beacons, operating in different frequencies and transmitting different patterns of pulses. Consequently, in order to achieve the goal of not being bounded to a particular underwater acoustic transmitter, the method to apply in this system has to be prepared for a scope of different frequencies.

3.1 TDOA Algorithm

The time difference of arrival (TDOA) technique has been extensively used for passive acoustic source positioning as discussed in section 2.4. The first approach was to analyze the pair of signals in the Matlab software and to analyze sets of real signals acquired in the test tank to identify features of the signals in the time domain that would be helpful for determining the TDOA. The duration of the signal transmitted by the beacon is 12 ms, but because of the reflection in the walls and the bottom of the tank, the significant length of the signals received was of approximately

80 ms. As referred in section 2.2.3, the underwater acoustic channel produces a lot of distortions, which in this confined environment are essentially due to the multiple reflections. This is a pessimistic, although possible, underwater acoustic scenario. One primary objective was that the system should be able to deal with such signals. These signals enhance the simulation for more robust algorithms that can work in rough situations. In figure 3.1 (top), the signals of the independent hydrophones are plotted. These signals were recorded with the transmitter aligned with the axis of the hydrophones, so that the time difference of arrival was the maximum possible. Considering the speed of sound in fresh water of $1482\,\mathrm{m\,s^{-1}}$ and the distance between the hydrophones of 6 cm, the delay expected is approximately 40.5 µs to the hydrophone-1 receive the signal previous in hydrophone-2.

Ideally, the distance between the hydrophones should be less than half of the wavelength (21.2 mm) to disambiguate the period of the transmitted signal. As this was impossible due to physical hydrophone size, the solution was to add one wavelength of the transmitted signal to the separation of the hydrophones, so the value of 6 cm.

One of the most popular methods to measure the phase shift is the generalized cross-correlation (GCC) process, so this was the first method to be evaluated. The data described above is analyzed in the following section.

3.1.1 Generalized Cross-Correlation

As referred in section 2.4, the generalized cross-correlation method is highly adopted to measure the time difference of arrival, because of its properties in masking the contribution of the ambient noise.

The process of determining the delay consist in calculating the correlation function of the two received signals. The result is a relation between the similarity of the two series with the lag relative to one another. The peak position of the correlation function indicates the instant in time where the signals are best aligned.

Figure 3.1 shows the two 35 kHz signals recorded in the test tank, where the red plot represents hydrophone-1, which is farther than hydrophone-2 (blue plot) in relation to the acoustic transmitter. The amplitude envelope is very dissimilar and highly variable with small displacements of the relative position of the two hydrophones. Because of this, the cross-correlation method is not useful in such situations. Figure 3.2 represents the correlation between the signals recorded. Measuring the time difference between the signals as the time position of the peak value of the cross-correlation function, the result is -1265 µs, which is clearly wrong based on the values previously calculated for the delay. As expected, the cross-correlation in the whole duration of the signal does not allow to have the correct estimation of the delay.

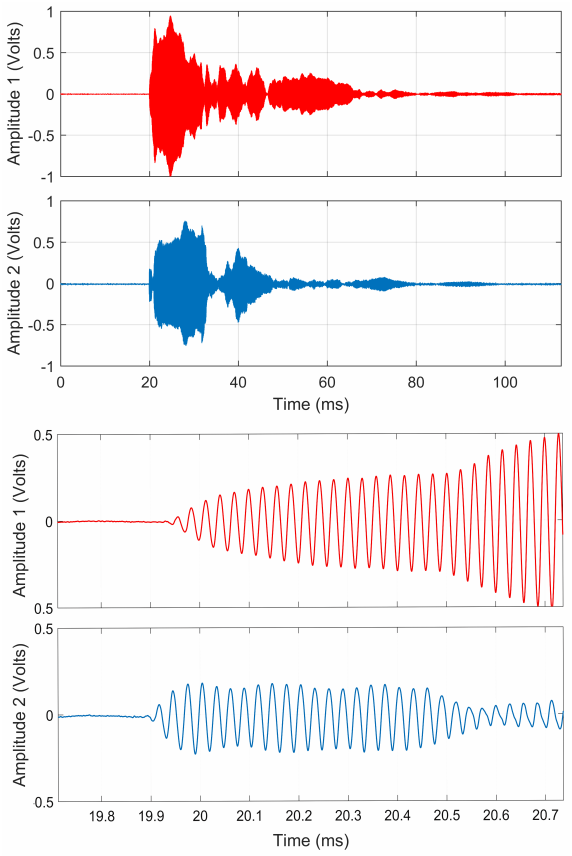

Figure 3.1: The 35 kHz signals recorded in experimental tests (top). Close-up in the beginning of the signal (bottom).

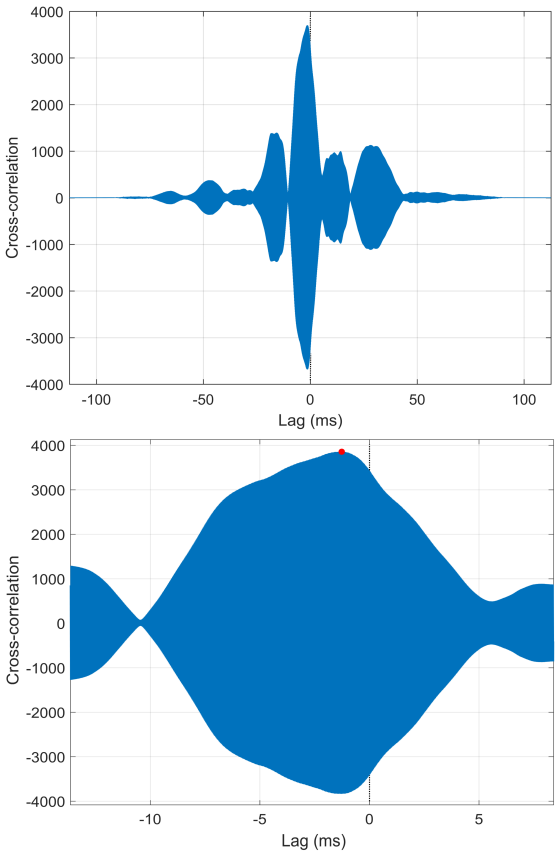

Figure 3.2: The result of the cross-correlation of the signals in figure 3.1 (top). Close-up in the peak of the correlation (bottom).

Generally, the signals are correlated with their entire significant duration, which can be difficult to do in real-time on long signals with high sampling frequencies and using low performance computing systems, due to the substantial computational effort needed.

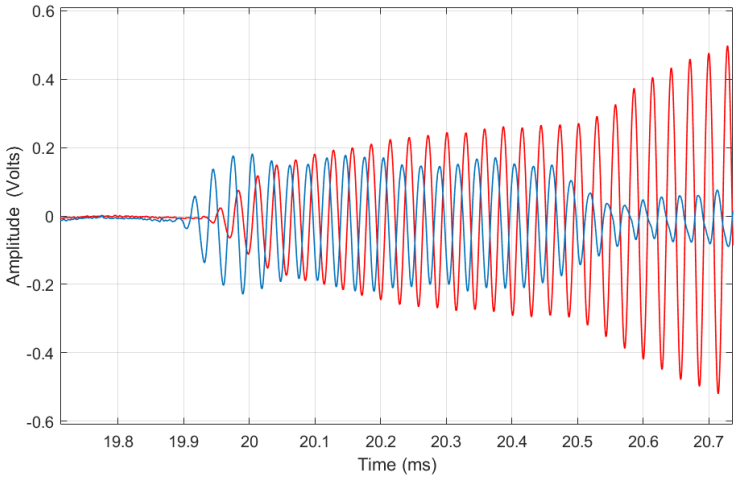

Figure 3.3: The beginning of the signals, hydrophone-1 red, hydrophone-2 blue.

An alternative approach is the segmentation of the signal in small portions and then applying the cross-correlation, as this requires a lighter computational effort and can produce better results.

Analyzing the beginning of the signal, as shown in figure 3.3, it is easy to notice the 35 kHz sine wave and the relative phase shift between the different received signals. The plot of the hydrophone-1, in red, is clearly delayed with respect to hydrophone-2 (blue) and it is clear that the delay is slightly higher than the period of the sinusoidal wave.

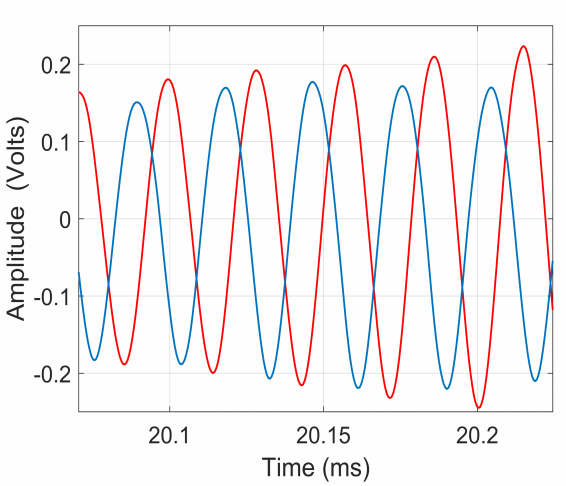

Figure 3.4: A fraction of the recorded signals shown in figure 3.3.

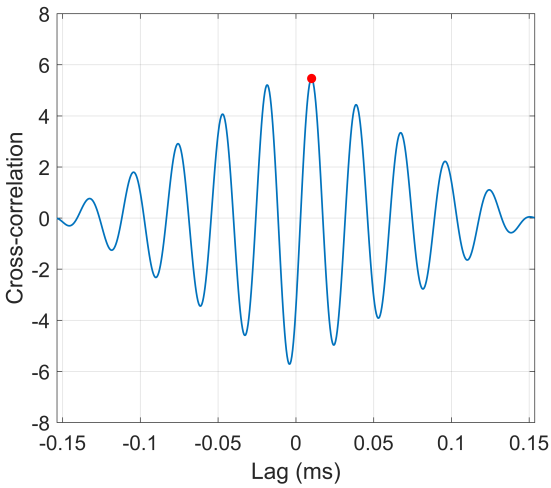

Figure 3.5: The result of the cross-correlation of the signals in figure 3.4.

The cross-correlation between sinusoidal waves has several peaks that correspond to delays that match the period of the wave, as shown in 3.5. Therefore, it is not plausible to determine delays above the period of the wave with cross-correlation method analyzing fractions of the signal.

Figure 3.4 shows a small fraction of the beginning of the signal, the result of the cross-correlation of the two signals is shown in 3.5. The maximum lag peak in this correlation occurs when the delay is approximately 10 µs, which, when added one period of the sinusoidal wave (nearly 29 µs), the result is 39 µs, what is close to the expected delay of 40.5 µs.

This process is acceptable for measuring the delay within a period, but in this case, the phase-shift is higher than the period of the wave, thus, creating an ambiguity that cannot be determined with this method.

Exploring the cross-correlation in small fractions of the signal it was concluded that the phase difference is not constant, because of the echoes that are added to the direct wave, provoking distortions in amplitude and especially in phase. Consequently, in order to successfully measure measuring the delay of arrival, the analysis has to be focused only on the beginning of the signal, where it is not influenced by the replicas.

Figure 3.6 shows the result of the cross-correlation of the start of the signals represented in 3.3. This function also cannot determine the true delay, because of the dissimilarity between the signals amplitude, giving a lag much higher than the expected, in this case 239 µs. For that reason, the analysis of the beginning of the signal has to be independent of the amplitude.

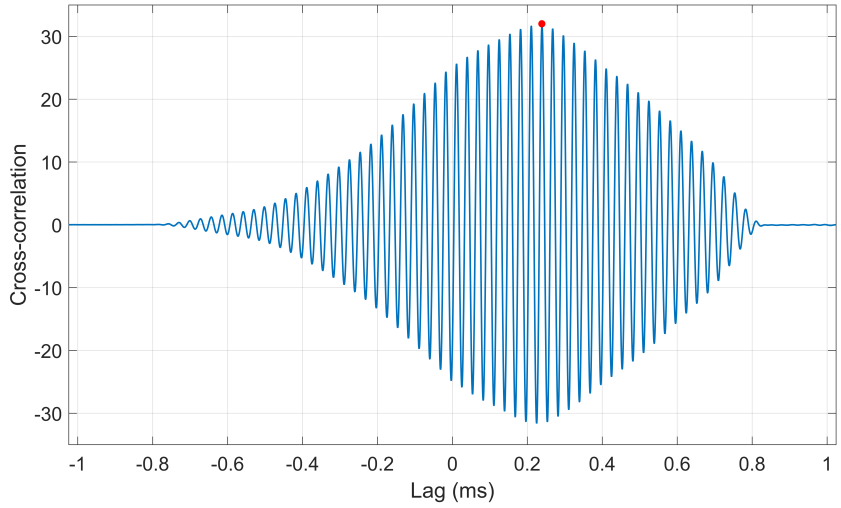

Figure 3.6: The result of the cross-correlation of the signals in figure 3.3.

3.1.2 Zero-Crossing Methodology

As discussed before, the method to measure the TDOA has to analyze the beginning of the signal, because all of the rest is affected by distortions, and it also has to be indifferent to the amplitude and the period duration of the wave. In this regard, the algorithm has to determine the instant of arrival of the two signals and then calculate the time difference between them. The focus has to be in accurately detecting only the very beginning of each received signal, analyzing them in the time domain.

The process is based on continuously detecting the zero-crossings of the signal and measuring the signal period as the time difference between two consecutive zero-crossing in the same direction (either rising or falling). A series of consecutive zeros occurring within a predefined time interval, the expected signal period, indicates the beginning of the received signal.

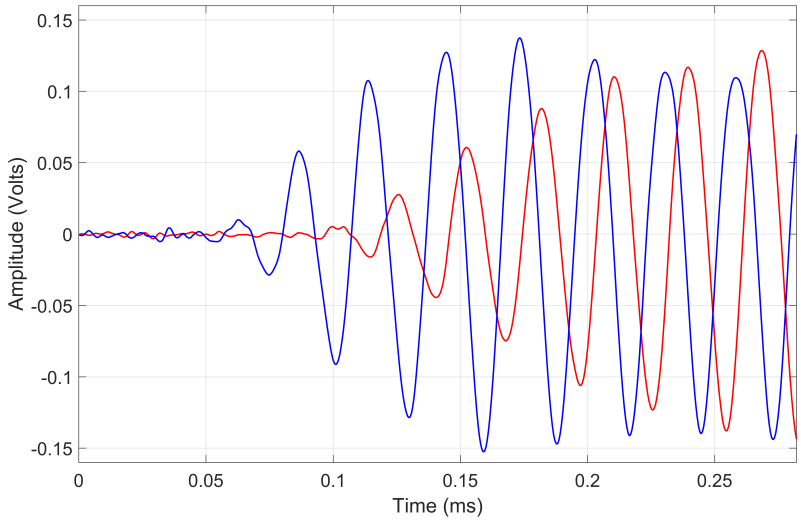

Figure 3.7: The beginning of the signal after filtering.

To improve the measurements of the zero-crossing periods it was decided to use a high-pass filter, to smooth the low-frequency components of the signal noise and eliminate any constant offset. For this, a high-pass filter with a cutoff frequency of 34 kHz was designed in Matlab, close to the transmitter frequency.

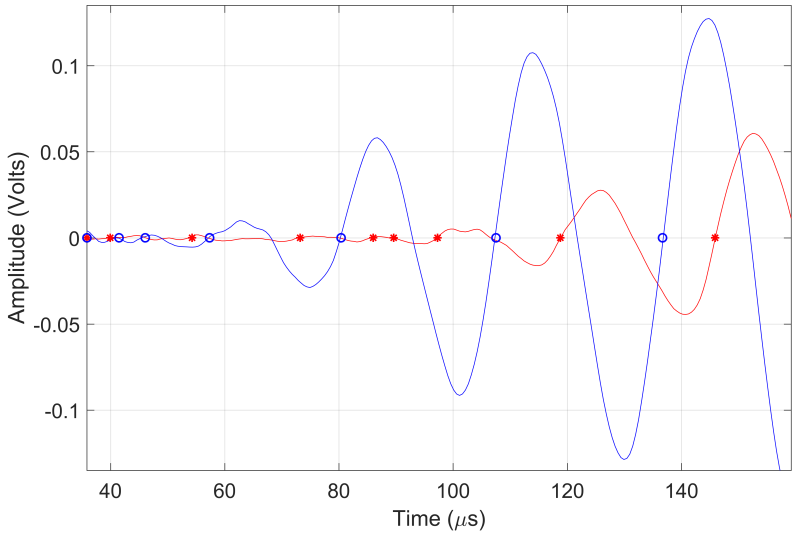

Figure 3.8: A close-up in the beginning of the signal of figure 3.7 after the zero-crossing detection (rising-edge).

The algorithm was developed and simulated in the Matlab software, applying the same recorded signals as before. Figure 3.7 represents a close-up at the beginning of the two signals in 3.3, after passing through the high-pass filter referred above, this figure is the reference for the next plots. Figure 3.8 is a close analysis of the previous figure,where the $*$, in red, exhibit the rising-edge zero-crossings of the signal recorded by the hydrophone-1, and the $\circ$ for the hydrophone-2, in blue. The method finds the pair of samples that cross zero in a rising mode, therefore, the first sample is negative, and the second one is positive, then, it chooses the closest sample to zero.

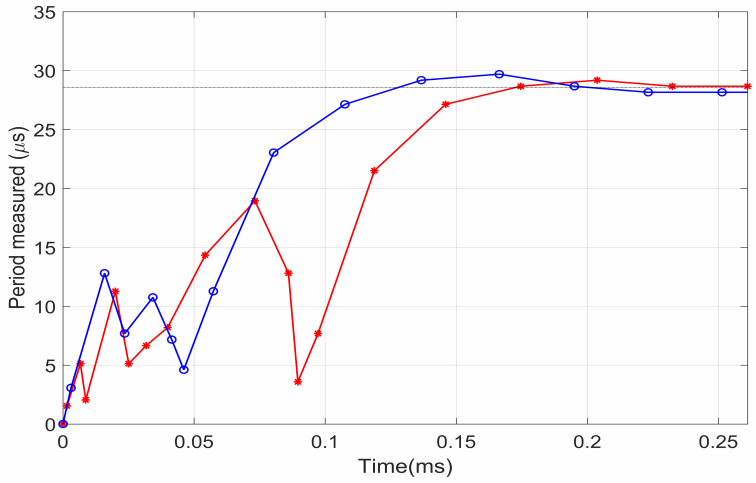

Figure 3.9: The period between the consecutive zeros in figure 3.7.

In the detection of the zeros, this method also measures the time difference between the consecutive zeros. Figure 3.9, is represented the period between the consecutive zeros in the y-axis, and the x-axis is the time with the same window as of figure 3.7. In this plot, it is possible to observe that after the signal arrival the period converges to the expected 28.6 µs (black dashed horizontal line), and that the signals merge to the period in different instants in time. When a small number of consecutive periods of both signals (typically between 5 and 20 periods) are detected above a threshold, the two signals are considered as arrived.

Towards the detection of the instant of arrival of both signals, it is necessary to further analyze the signal zeros closer to the decision threshold and measure the TDOA as the time difference between them, as shown in figure 3.10.

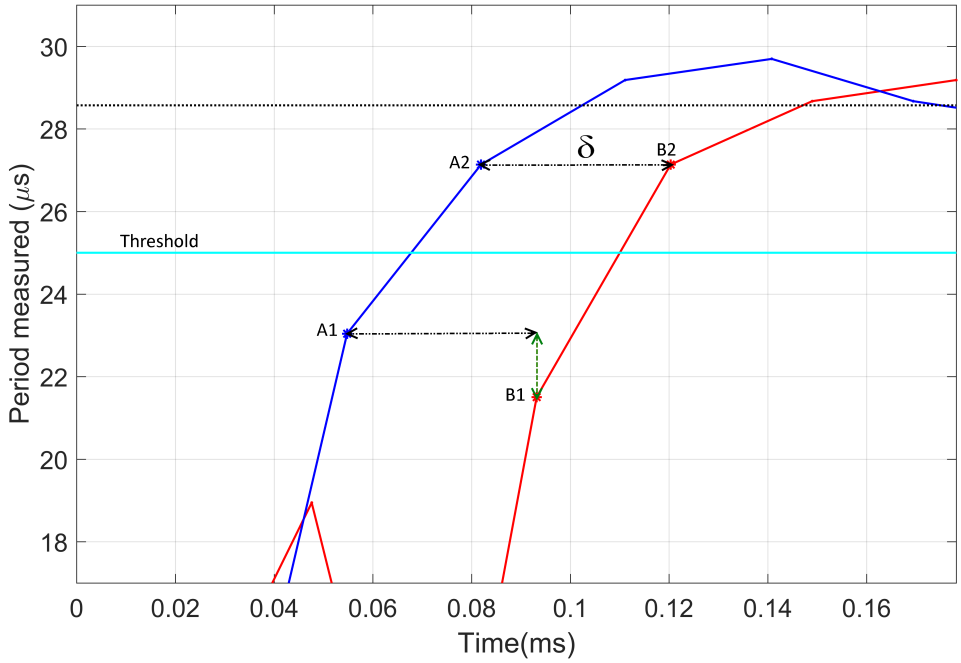

Figure 3.10: Analysis of the zeros period around the threshold.

This examination has to be made in the transition to the nominal period to catch the first zero of the beginning of the signal, so, the threshold has to be lower than the expected period, but higher than the zero periods of the noise. Simulation experiments have shown that using threshold values between 75% and 95% of the nominal period, the TDOA results calculated, match the expected time delay for different angles.

For choosing the zero that represents the beginning of the signal, the zero before and after the threshold in both hydrophones are analyzed. In figure 3.10, the zeros of the hydrophone-2, the blue plot, are the points *A1* and the *A2*, corresponding to the zeros before and after the threshold, for the hydrophone-1, it coincides with the points *B1* and the *B2*, in red. The algorithm has to match the same zero in both signals to correctly estimate the delay, so, it measures the period difference between the zeros in distinct plots. The difference between the *A1* and the *B1* is represented by a

green vertical line, in figure 3.10. It also determines the difference for the other combinations, like *A1-B2*, *A2-B1*, and *A2-B2*. Then, it chooses the one that minimizes the difference, in this case, the *A2-B2*. Afterwards, it can measure the time difference between the zeros, represented by δ in the figure. The value measured was 38.4 µs, which is near to the theoretical value of 40.5 µs. The difference can be justified by the error in the distance between the hydrophones or the inaccuracy in measuring the experiment angle.

The algorithm was validated with different recorded signals, in various angles, using the same approach. In chapter 5, the results are discussed using this method, with a variety of distinct configurations.

3.2 DOA Determination

After measuring the time difference of arrival, it is feasible to calculate the direction of arrival (DOA), towards tracking the acoustic transmitter. As presented in section 2.5, there are two primary methods to determine the DOA, and both are dependent of the hydrophones spatial configuration.

In this work, it was only used two hydrophones, which simplifies the determination of the angle, but confines it only to two dimensions. The first approach considered was the trilateration method.

3.2.1 Trilateration

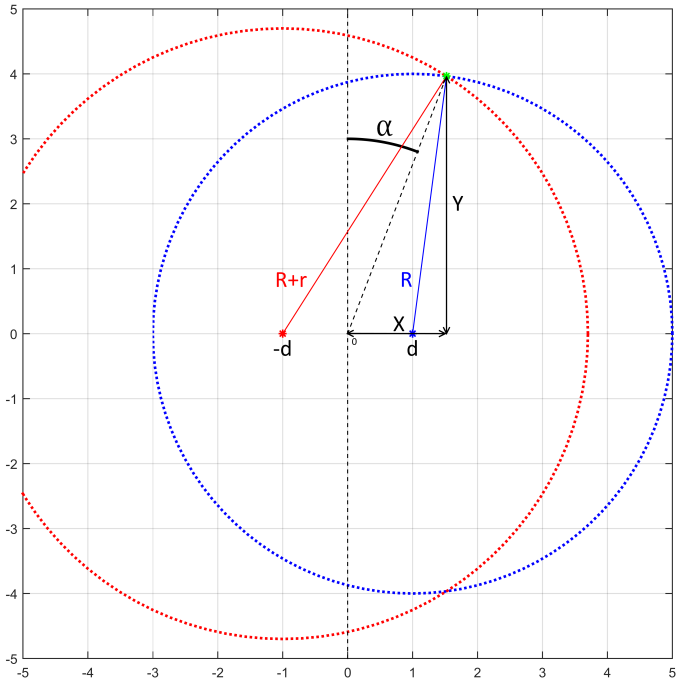

Figure 3.11: The two dimensions spatial configuration of the hydrophones and a beacon for trilateration.

In two dimensions, the trilateration method consists in finding the intersection between two circles, in figure 3.11 is represented the spatial configuration of the problem. The red point is hydrophone-1, the blue is hydrophone-2, and the green point is the acoustic transmitter. With this configuration it is only possible to determine the direction (azimuth) of the transmitter along the horizontal plane where the receivers are located, and thus the elevation (corresponding to the vertical angle) is undetermined, figure 2.6 shows this angles. In this work we will only consider the determination of the azimuth with the two hydrophones, although adding one more hydrophone would allow the elevation ambiguity to be resolved.

The distance between the transmitter and hydrophone-2 is **R**, the distance between hydrophone-1 and the target is **R+r**. These distances, are the radius of the circles, whose centers are the hydrophones. The **r** is the time difference of arrival multiplied by the speed of sound in water.

A distance of **2d** separates the hydrophones, and the center is the referential of the system. The goal is to determine the distances **X** and **Y** and then the angle α. This angle is 0° when the transmitter is in front of the hydrophones (the vertical dashed line in figure 3.11) in line with the referential. It varies from -90° to 90°, from left to right correspondingly. It is impossible to know if the transmitter is in front or behind the hydrophones because there are always two points of intersection of the two circles, unless the angle is 90° or -90°.

To determine the intersections of the circles, it was necessary to solve the system of equations of the two circles in order of **X** and **Y**. The first equation in 3.1 is for the red circle, centered on hydrophone-1 and the second one is for the blue circle, centered on hydrophone-2.

$$\begin{cases} (R+r)^2 &= (X+d)^2+Y^2 \\ R^2 &= (X-d)^2+Y^2 \end{cases} \tag{3.1}$$

Solving symbolically the equations shown in 3.1 yields the equations 3.2, where **X** and **Y** represent the Cartesian coordinates of the circles intersection. Then, using trigonometry, the angle α is determined in 3.3.

$$\begin{cases} X &= \dfrac{r(r+2R)}{4d} \\ Y &= \pm\dfrac{1}{4}\sqrt{\dfrac{-16d^4+8d^2r^2-r^4+16d^2rR-4r^3R+16d^2R^2-4r^2R^2}{d^2}} \end{cases} \quad ,d \neq 0 \tag{3.2}$$

$$\alpha = \arctan\left(\frac{X}{Y}\right) \tag{3.3}$$

In this context, **d** (the hydrophone distance to the center) and the **r** (variation in the distance cased by the TDOA) are known, but **R** is undetermined because this system does not measure the

range. In figure 3.12, it is shown the variation of the TDOA, which is proportional to **r**, and the correspondent angle of arrival, α. In this plot, the distance considered between hydrophones was 6 cm and the distance between the transmitter and the closest hydrophone was 10 m.

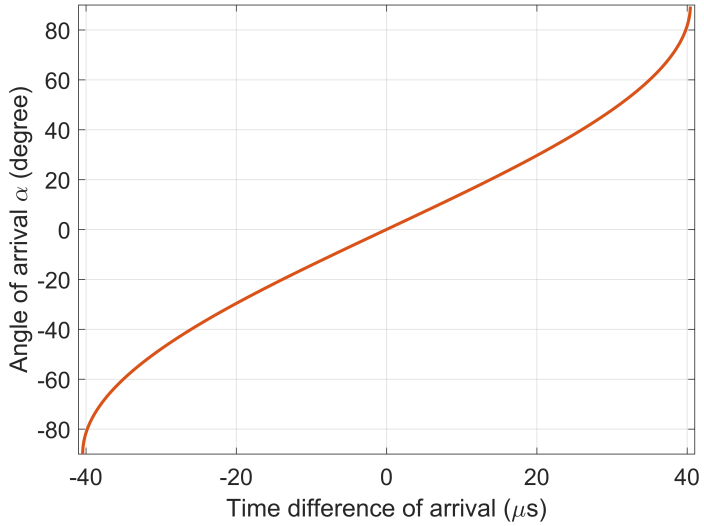

Figure 3.12: The angle of arrival due to the TDOA.

For the same TDOA the angle changes with the distance **R**, but as shown in figure 3.13 the variation is too insignificant. In this plot, it is represented the absolute maximum difference of all the possible angles α, calculated with a **R**=1 m, and the angles with the increasing **R**.

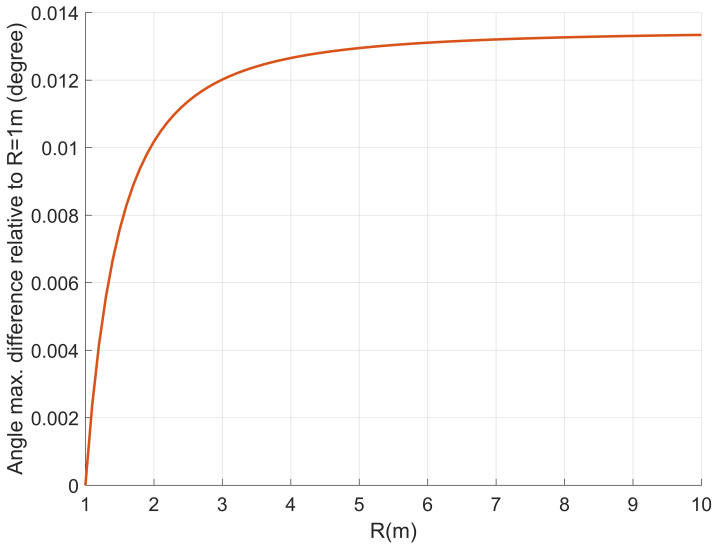

Figure 3.13: The maximum difference of the angle α for variations in **R**.

This method can determine the angle of arrival without knowing the **R**, but considering realistic scenarios where the distance d between the hydrophones is much smaller than the distance to the

acoustic source. As shown in figure 3.13, the error in the angle for not considering the actual value of R (or assuming R $\gg$ d) stays under 0.02°.

3.2.2 Multilateration

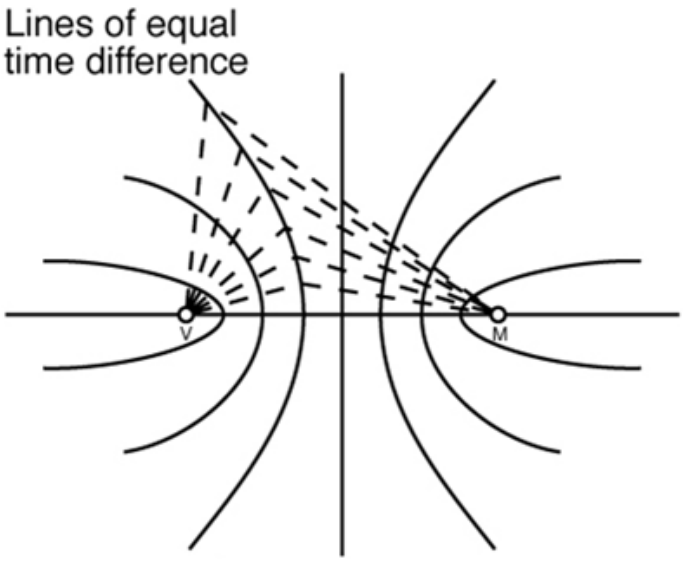

Figure 3.14: Diagram illustrating multilateration.

The multilateration technique can determinate the angle versus TDOA as well. This method is based on hyperbolas, as shown in figure 3.14, that describe all the possible locations of the transmitter with the a given TDOA. Equation 3.4 describes this hyperbola, where **r** and **d** are the same as the trilateration diagram shown in figure 3.11. The equations presented were determined in the Dalskov and Olesen (2014), and the hyperbola equation is shown below.

$$y(x) = \frac{1}{2}\sqrt{\frac{(4x^2 - r^2)(4d^2 - r^2)}{r^2}} \tag{3.4}$$

If it is assumed that the sound source is at a much larger distance than the separation of the hydrophones, the approximation of the wave to a plane is reasonable. Therefore, in this case the direction of propagation coincides with the asymptote of the hyperbola, and the angle of arrival can be determined by the slope of the asymptote. The asymptote is defined by the equation 3.5.

$$y(x) = x\frac{\sqrt{4d^2 - r^2}}{r} \tag{3.5}$$

Adapting the angle of the asymptote to match the trilateration plot configuration, the result is the system of equations in 3.6.

$$\alpha = \begin{cases} -90 - \arctan\left(\dfrac{\sqrt{4d^2 - r^2}}{r}\right) & , r < 0 \\ \\ 90 - \arctan\left(\dfrac{\sqrt{4d^2 - r^2}}{r}\right) & , r \geq 0 \end{cases} \tag{3.6}$$

As shown in the plot of figure 3.15, the difference between the two methods, under the assumptions taken (R $\gg$ d) is negligible. With these results we can conclude that it is much simpler to compute the angle of arrival using the multilateration technique.

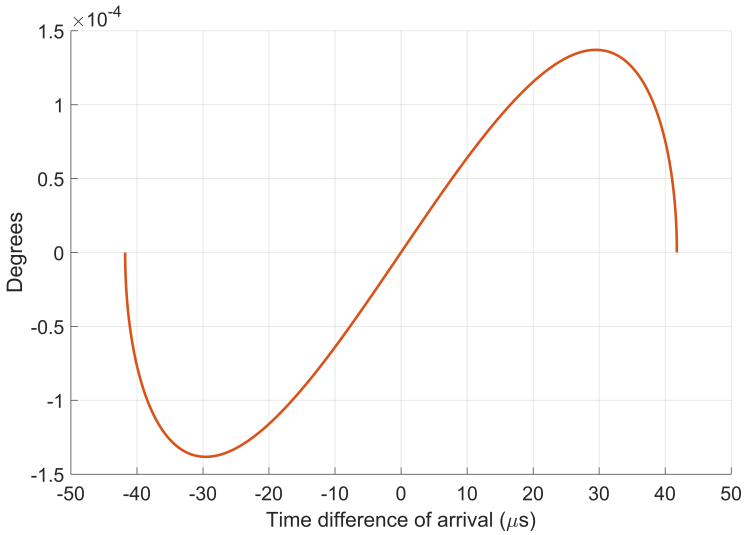

Figure 3.15: The difference between the trilateration plot in figure 3.12 and the equivalent calculated by multilateration.

Summary

In this chapter, several simulations were made to find the best suitable algorithm to determine the time difference of arrival, was discussed the generalized cross-correlation and a different strategy proposed in this work, the zero-crossing method. By analyzing two different methods to determine the angle of arrival with the time difference of arrival, we concluded that both methods were equivalent for the conditions considered in this work.

Chapter 4

Implementation

This chapter starts by describing the electronic systems used in this work, from the underwater acoustic beacon to the receiver analog front-end and embedded computing platform. Then, the implementation of the algorithm described in section 3.1.2 for determining the TDOA is presented, as a dedicated hardware peripheral. Lastly, the software implementation to calculate the direction of arrival, that runs on the embedded processor is shown.

4.1 Hardware Equipment

4.1.1 Transmission

As referred in the previous chapters, we decided to use an underwater commercial acoustic beacon to serve as the transmitter because of their robustness, and easy applicability in several different scenarios. There are various different similar devices available in the market with diverse characteristics like range, depth, frequency, and autonomy.

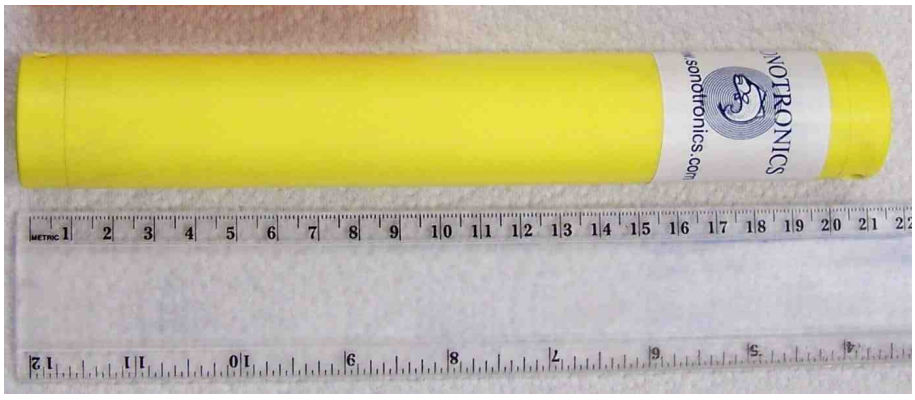

Figure 4.1: The Sonotronics Inc., *EMT-01-03*, underwater acoustic beacon.

The one available for this work was an *EMT-01-03 Equipment Marking Transmitters*, from *Sonotronics*, usually used to attach to submerged equipment in order to locate it in case of loss. This is generally employed with a dedicated acoustic receiver tunable in the beacon's frequency,

with an announced maximum usable range of 4 km. As figure 4.1 shows, the beacon is a tube with 210 mm of length, 32 mm in diameter, and weights in air 223 g. The EMT-01-3 has a replaceable battery and is rated for a maximum depth of 1000 m.

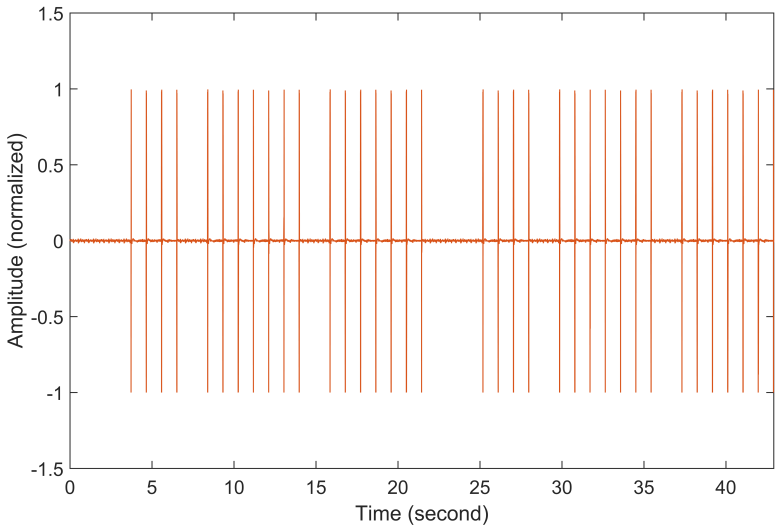

Figure 4.2: Recording of the beacon acoustic pattern.

This beacon emits a periodic signal that consists of a series of short sinusoidal pulses with a frequency of 35 kHz, each one lasting about 12 ms. Every beacon has its own periodic pattern, the one employed as a 4-8-8 pattern that is shown in figure 4.2. The time interval between consecutive pulses is 930 ms, and the other separation intervals are 1860 ms and 3720 ms. One complete patterns lasts for approximately 23.5 s and contains 20 identical pulses.

4.1.2 Reception

Recording device

The acquisition of the acoustic signals propagated in the water is made by a pair of omnidirectional hydrophones. The ones used are from the company *Aquarian Audio Products*, and the model is the H2a hydrophone. The interface with the recording device is a 3.5 mm microphone input. In figure 4.3, the hydrophones are shown in a structure built to fix them at a distance of 6 cm apart. The dimensions of the hydrophones are 25 mm $\times$ 46 mm, which makes it impossible to be at a distance of less than 25 mm. As this distance is superior to half of the wavelength (21.2 mm) of the transmitted signal, it is not possible to measure the TDOA by the phase difference between the two signals. We decided to use a distance between the hydrophones slightly below 1.5$\times$ wave length for an easy support construction.

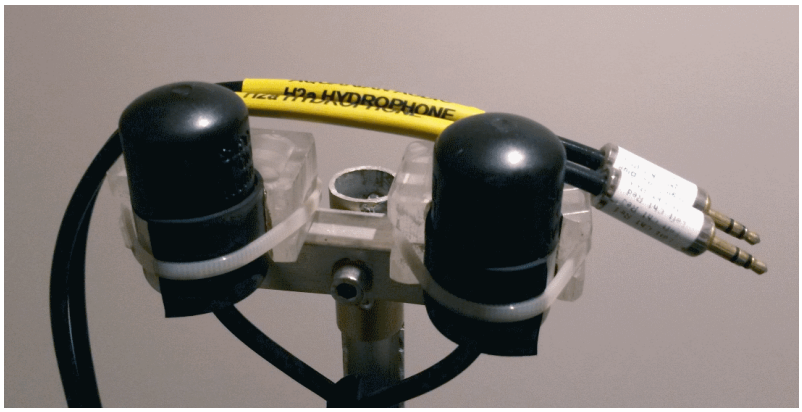

Figure 4.3: The structure holding the two hydrophones 6 cm apart.

Analog front-end

The hydrophones are connected to a custom designed analog front-end board with a variable gain amplifier and low-pass anti-aliasing filtering. The analog pre-processing applies two variable and digitally controllable amplifiers chains, one for each hydrophone, followed by analog low-pass anti-aliasing filters with a cutoff frequency set to, approximately, 250 kHz. This board also includes a high-speed analog switch, allowing to multiplex two additional analog signals by using a second amplifier and filtering board. The amplifier chain is divided into two stages, the first one with a gain adjusted to 10×, and the second stage with two I2C digital potentiometers that allows programming the gain of two analog amplifiers in series with an overall gain that varies from 0.1× to 2500×. Figure 4.5, shows the analog front-end board in the right side, and figure 4.4 presents a simplified block diagram of one amplifier and filtering analog path.

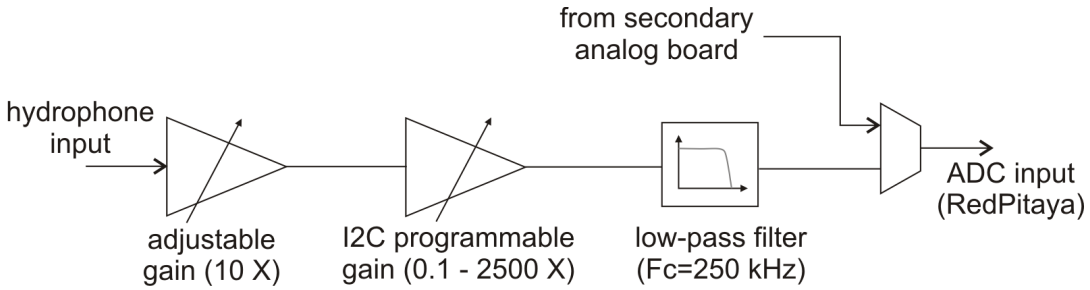

Figure 4.4: A simplified block diagram of the analog programmable amplifier and filtering daughter board.

Digital platform

The digital platform used to process the signals was the RedPitaya single board computer, based on the XILINX Zynq 7010 programmable SoC (figure 4.5 left). This device integrates a dual core ARM Cortex A9 with a peripheral FPGA fabric for the integration of custom designed co-processing or interfacing blocks. Besides, the standard on-board interfaces and devices required to

run a Linux operating system (DDR memory, Ethernet interface, SD flash memory and USB), this board also includes a dual high-speed ADC and a dual high-speed DAC, both capable of operating at a sample frequency of 125 Msps. This platform is usually sold as an all-in-one laboratory instrument, providing the programmable logic (PL) hardware interfaces and web applications that implements an oscilloscope, an arbitrary function generator, a spectrum analyzer and also a general purpose PID controller. The hardware design for the PL section is provided as an open source project for the XILINX Vivado design tool suite. A variant of the original hardware system also includes a DMA controller that allows the continuous acquisition and recording of the two analog input signals up to 2 Msps.

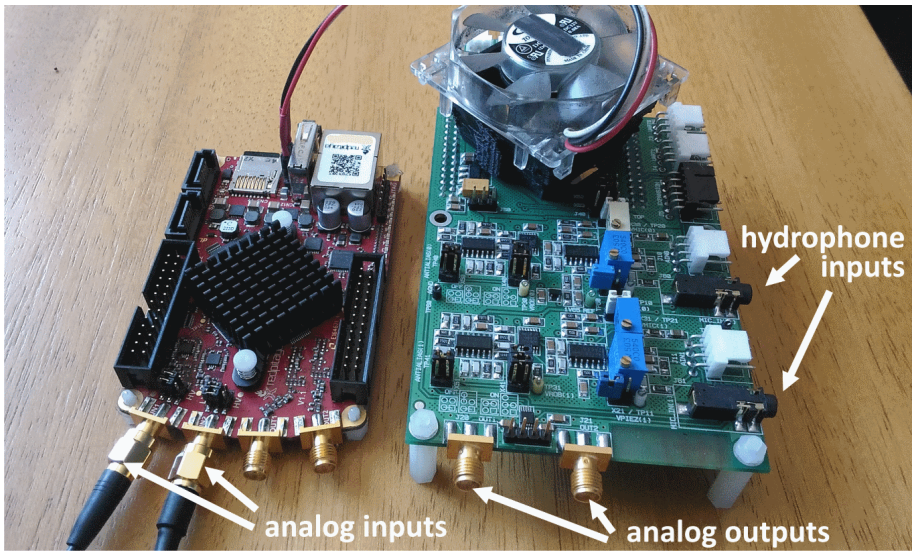

Figure 4.5: The RedPitaya embedded computer (left) and the analog front-end amplifier board (right).

4.2 Digital Implementation

System Integration

The re-programmable hardware system was based on the original design included in the RedPitaya distribution, maintaining the parts that implement the oscilloscope and the continuous signal recording, and removing all the other unused modules to free FPGA resources and facilitate the design optimization process to reach the 125 MHz main clock frequency. The oscilloscope function is very convenient for debugging when performing field experiments, by analyzing the real signals being captured by the acoustic sensors. The input to the module implementing the oscilloscope is taken from a configurable decimator module that reduces the sampling frequency by factors equal to powers of two and averages the samples, which is used by the oscilloscope application to adjust the timebase. The oscilloscope can be accessed by an internet browser when the RedPitaya is on the same network, providing a graphic interface for analyzing the signals.

The TDoA calculator was integrated in the original oscilloscope interface (figure 4.6), keeping the whole original functionality. To further enhance this, a multiplexer has been added to the oscilloscope datapath, for being able to use that same circuit and software application for observing other intermediate signals in different points of the TDOA determination.

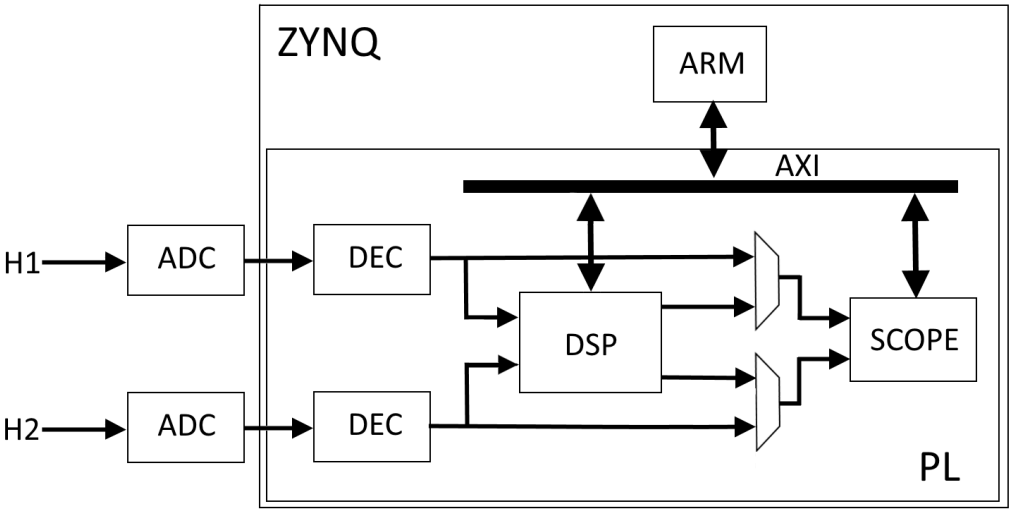

Figure 4.6: Simplified block diagram of the top-level module.

The ARM processor shares data with the FPGA using the AXI interface, enabling a fast communication link between the Linux OS and the re-programmable hardware. This connection is used for configuring the modules parameters in real-time and transmitting the relevant data to the post-processing unit.

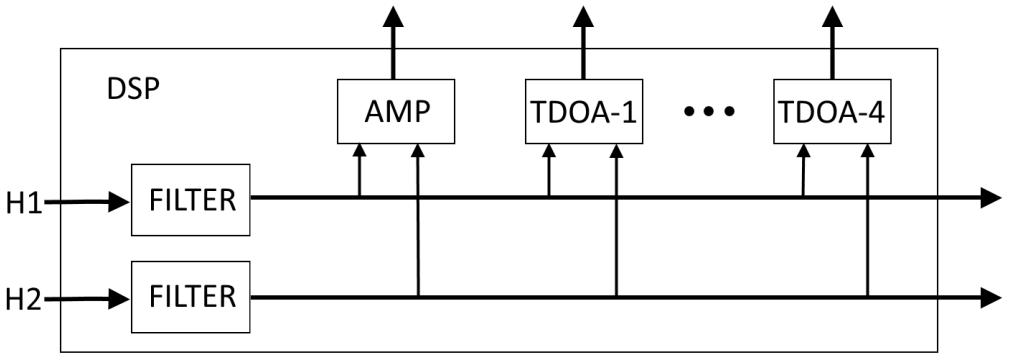

Figure 4.7: Simplified block diagram of the DSP module.

A simplified block diagram of the top-level module on the Programmable Logic (PL) device and their interfaces is shown in figure 4.6. The output of the analog front-end for each hydrophone (H1 and H2) is connected to the analog to digital converter (ADC), then passes through the decimator (DEC) and enters the digital signal processing (DSP) unit, that contains all of the modules that implement the TDOA calculator.

The DSP module is represented in a simplified diagram in figure 4.7. The next subsections will describe the three different modules in more detail.

High-pass filter

The signal from each channel passes through a digital high-pass filter with a cutoff frequency of 34 kHz to attenuate the low-frequency components.

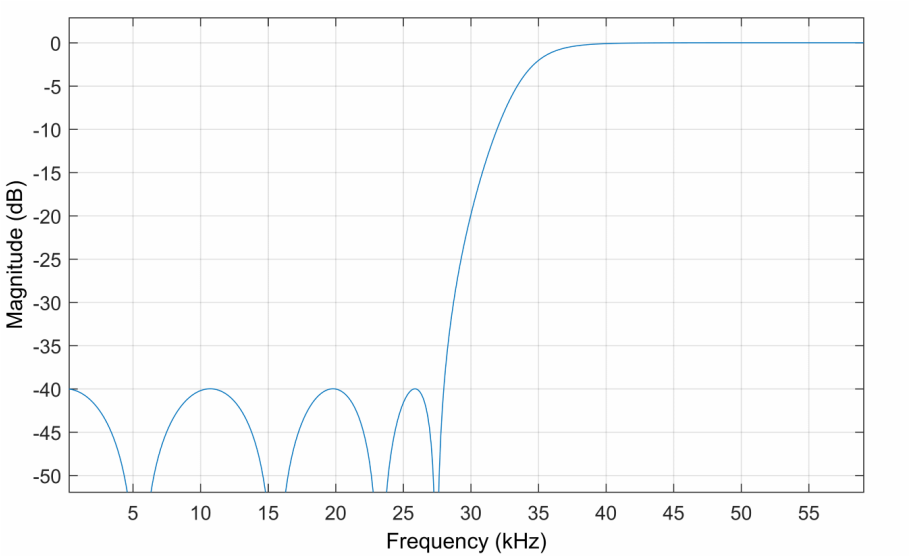

Figure 4.8: Magnitude response of the high-pass filter.

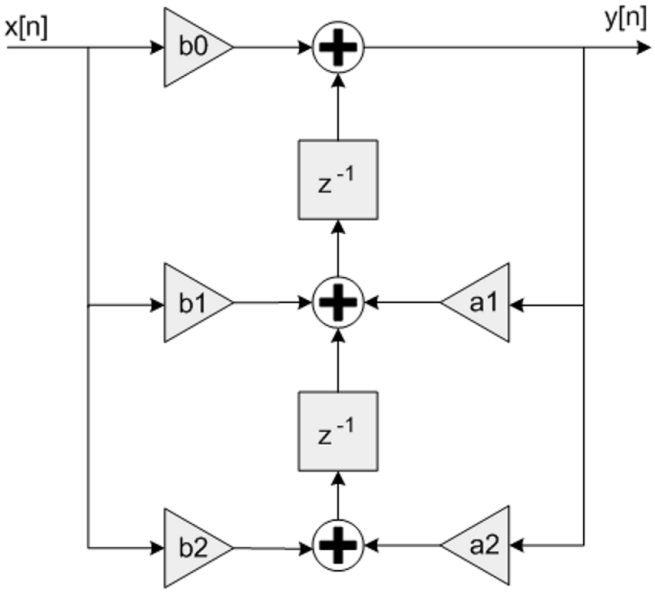

Figure 4.9: Diagram of the transposed Direct Form II Biquad.

The filter was designed in Matlab to perform a type II Chebyshev infinite impulse response filter (IIR). As shown in figure 4.8, the magnitude response has no ripple in the pass-band but does

have equiripple in the stop-band below 28 kHz, with an attenuation of 40 dB. It was chosen an IIR topology to save resources but maintaining a high roll-off. The filter of order 8 was implemented in four biquads, direct form II transposed structure, and connected in cascade, the topology of the biquad is shown in figure 4.9. These decisions were made to prevent instability and the overflow of the signal. Using the filter design and analysis tool (FDATool) in Matlab is feasible to extract the coefficients (b0, b1, b2, a1, a2) for applying directly in the structure in figure 4.9.

Amplitude Determination

The AMP block in figure 4.7 is an amplitude measurement module that determines the maximum amplitude of each signal over a configurable time window. This information is then transferred to the ARM processor for later analysis, the time in which the amplitude is inspected, it is also configurable by the ARM.

TDOA Calculator

The DSP instantiates four TDOA calculators with different configurations that the post-processing unit can change in real-time, the delay measurements are passed to the ARM for future analysis. The filtered signal is also forward to the oscilloscope for the analysis in the web application.

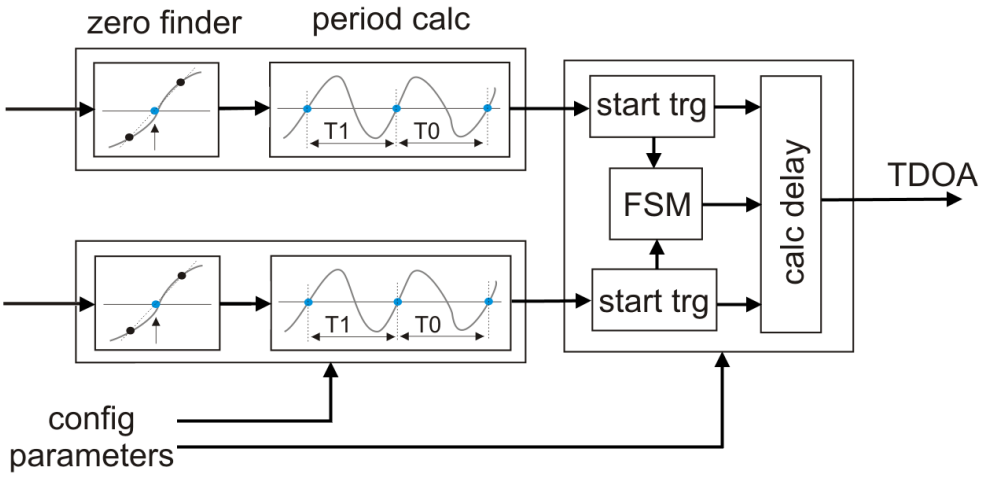

Figure 4.10: Simplified block diagram of one TDOA calculator. Four modules are instantiated with different parameters.

The TDOA calculator module is shown in figure 4.10. Each of the four modules receives the signals of two hydrophones (H1 and H2), after passing through the decimator and high-pass filter, as shown in figure 4.7. The signal is then forwarded to the zero finder block, which is calculated continuously the time difference between two consecutive transitions by zero in the same direction (the rising edge in the block shown), measuring the period of the input signal. The sequence of periods of each signal is analyzed to detect a number of consecutive valid periods whose duration is above the threshold, as explained in section 3.1.2. This is the trigger event that indicates the

start of that signal. A finite state machine receives these trigger signals, analyzes the sequence of periods determined and drives the delay calculator module that estimates the TDOA, applying the method described in section 3.1.2.

Two of these modules are instantiated to find the signal period using rising edge transitions and the other two, the falling edge. A pair of modules containing the two different approaches share all the same parameters. The TDOA calculator measures the time delay between detecting the arrival of the signal in each hydrophone, if this time is higher than a maximum delay configuration, then the module activates a time-out flag. When the module detects the arrival of both signals or the time-out is flagged, it waits for a configurable time until starting analyzing the signal again. This is to ensure that the system does not inspect the signal in the continuous transmission and that it is prepared for the start of the next pulse.

4.3 Implementation Results

The implementation in the Zynq 7010 programmable SoC, maintaining the oscilloscope and the DMA interface for real-time recording, occupies the FPGA resources shown in table 4.1. The high utilization of the DSP slices is due to the pipelined implementation of the two high-pass IIR filters.

Resource	Occupancy
LUT	33% (5759)
FF	17% (6001)
BRAM	27% (16)
DSP48	83% (66)

Table 4.1: FPGA resource usage (Zynq 7010).

The development was done in the XILINX Vivado design tool and the simulation of the individual modules described above in the ModelSim software.

The simulation of the top-level module, shown in figure 4.6, was performed with the recorded signals used in the development of the algorithm in chapter 3.

Figure 4.11 shows the result of the simulation in the ModelSim, obtaining four delays that correspond to the four different TDOA calculators. The values obtained, match the expected delays simulated in MATLAB, for the signals and parameters chosen. The estimates are calculated after the modules receive 8 consecutive transitions by zero, as two of them analyze the rising edge and the other two the falling they update the delay in different instants in time. The configuration parameters were adjusted to the recorded beacon signal, as explained in section 5.1.

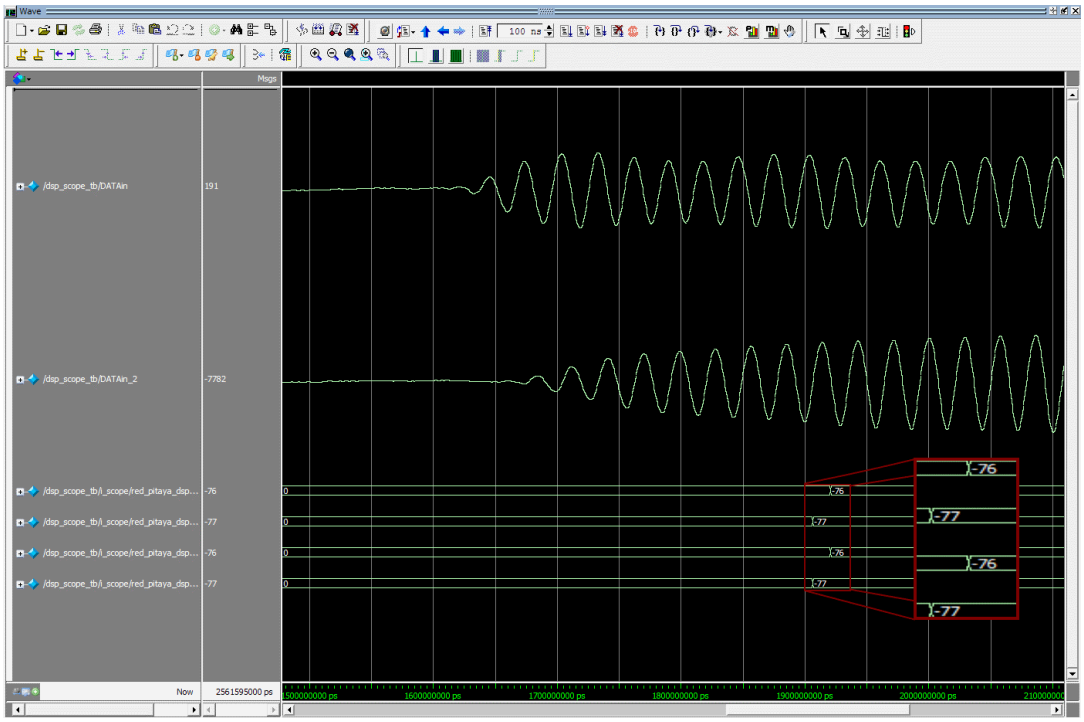

Figure 4.11: The result of the ModelSim simulation.

4.4 Software Processing

The ARM processor running Linux is the post-processing unit that connects with the FPGA. Taking advantage of the filesystem and the interfaces already developed was created programs, written in C (programming language), to control and analyze the data from the digital implementation.

Automatic Gain Controller

The signals recorded have amplitudes that are affected by the distance to the transmitter and can also be different between the hydrophones. To solve this was developed an automatic gain controller, which the goal was to change the gain of the amplifiers in the analog front-end to maintain the range of the signals regulated. As described in section 4.1.2, each channel as two digital configurable potentiometers that change the gain of the analog amplifiers, the input signal can be raised from $1\times$ to $25000\times$ the original amplitude. The C program uses the I2C digital interface to modify the gain. This is done by a proportional controller that adjusts the amplitude to 80% of the ADC maximum range. The greatest amplitude of the signal is determined by the FPGA module presented in section 4.2, the value is calculated over a period of time, then the amplitude is written in the shared memory and the module reseted. Every time the program has a new amplitude, updates the gain value for each channel. The time window used to measure the amplitude must ensure that capture of a significant part of the transmitted signal, in this case, a sine pulse from the beacon. This time can be configured by the program, and for the beacon described in section 4.1.1, it was chosen 5 s towards ensuring the capture of at least one pulse.

4.4.1 Implementation Parameters

Several parameters can be adjusted by the programs running on the ARM core. An enumeration of all the parameters that can be configured in real-time by the post-processing unit is shown below.

1. **Decimation factor** - power of two values between 1 and 65536.

2. **Scope input** - controls the multiplexer shown in figure 4.6, that can change the data going to the oscilloscope web application between original and filtered signals.

3. **Threshold-1** - adjusts the value in which the zero periods are considered correct from the expected signal. Changes the threshold in one pair of modules.

4. **Threshold-2** - the same as before but changes the threshold in the other pair of modules containing a rising-edge block and a falling-edge.

5. **Number of zeros** - number of transitions by zero to consider that the signal arrived.

6. **Maximum delay** - the highest delay between the arrival of both signals to signalized the time-out flag.

7. **Inactivity time** - the time period that the modules are disabled after detecting the signals beginning or time-out.

8. **Amplitude time** - the time period in which the gain module analyzes the maximum amplitude of the signal before updating the value and resetting.

DOA Determination

After the configuration of all the parameters, the application reads the four TDOA estimates and implements a series of filters to calculate the final TDOA. This process was enhanced by the analysis of the results retrieved in the laboratory experiments, in section 5.2.1. A more detail explication of the algorithm chosen is done in that section.

The TDOA value is then used to estimate the direction of the sound source using the techniques studied in section 3.2. Both approaches are computationally heavy for real-time calculations, therefore it was decided to fit the trilateration function with low order polynomial functions. The best match with the minimum error was a polynomial equation of third order from -60° to 60° with approximately 0.25° of deviation to the expected function (blue section in figure 4.12). Other two polynomial equations to match the function from the 60° to the 90° and other two symmetrical ones for the negative angles, with a maximum error of 0.57°.

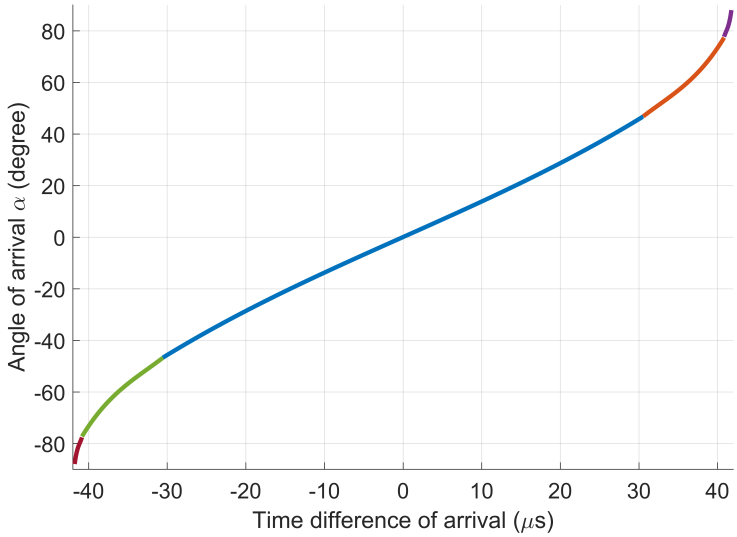

Figure 4.12: The polynomial functions that fit to the trilateration function.

Summary

This chapter presented the equipment used for the implementation of the algorithm and for the experimental tests. The hardware implementation was described in detail from the the analog front-end, to the FPGA modules, and the application running in the ARM-based unit. Explaining how the signal is processed since the recording until the determination of the direction of arrival.

Chapter 5

Practical Experiments

In this chapter, it will be presented the experiments done to validate this work. Starting with the parameters configuration of the hardware implementation, then the tank tests and interpretation of the results to enhance the post-processing analysis. Afterwards, the system was tested in the field with the goal of tracking the acoustic transmitter. The results are also presented in this chapter.

5.1 Parameters Configuration

As referred in section 4.2, the continuous acquisition by the DMA controller to record the two signals is limited to a sampling frequency of 2 MHz, so the decimation factor has to be higher than 64 for using the functionality to record continuous signals to the ARM flash disk. It was decided to use the maximum sampling frequency possible to have the best signal resolution, therefore, the frequency used was 1.953 125 MHz which is the result of dividing the ADC sampling frequency by the decimation factor, $\frac{125\,\text{MHz}}{64}$.

The number of zeros received to trigger the beginning of the signal was set to eight, because in the experimental test good results were obtained with values between 4 and 12.

The two configurable thresholds were 86% and 93.2% of the period of the transmitted signal because are whole numbers measured in sample periods and are between the working interval studied in the Matlab simulation, in section 3.1.2.

The maximum time difference of arrival was calculated by the separation of the hydrophones, in which it was added some room for not being a hard limit and accommodate all the uncertainty in the measures. Considering the speed of sound in fresh water of $1482\,\text{m}\,\text{s}^{-1}$ and the distance between the hydrophones of 6 cm, the delay expected is approximately 40.5 µs. The maximum delay between the arrival of both signals to signalize the time-out flag is the expected maximum delay plus some margin, so was chosen 51.2 µs that corresponds to 100 sampling periods.

The time period that the modules are disabled after detecting the signals is 200 ms which guarantees that the 35 kHz pulse and its replicas are finished.

The following table summarizes all the parameters needed to configure the FPGA modules for measuring the TDOA of the underwater acoustic beacon used.

Parameter	Value
Decimation factor	64
Threshold-1	86%
Threshold-2	93.2%
Number of zeros	8
Maximum delay	51.2 µs
Inactivity time	200 ms
Amplitude time	5 s

Table 5.1: Parameters configuration for experimental tests.

5.2 Laboratory experiments

The preliminary laboratory experiments were done in a test tank of fresh water, with 4.75 m by 4.4 m and 1.7 m of depth. The structure with the hydrophones was submerged 40 cm into water and the active beacon was placed at a distance of 2.5 m and immersed about 50 cm below the surface.

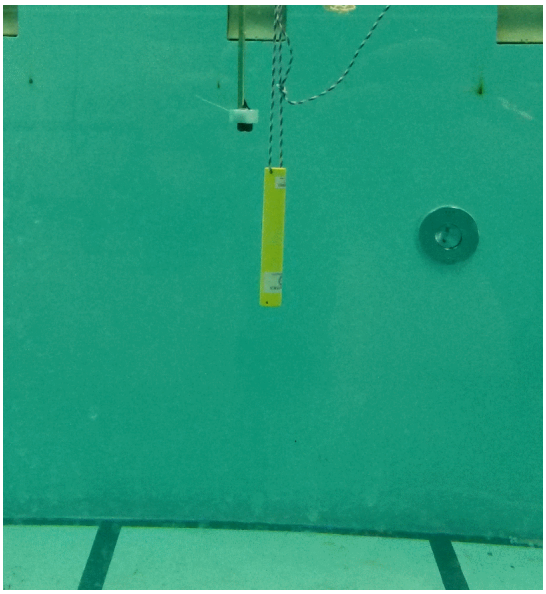

Figure 5.1: Underwater photograph displaying the beacon and the hydrophones.

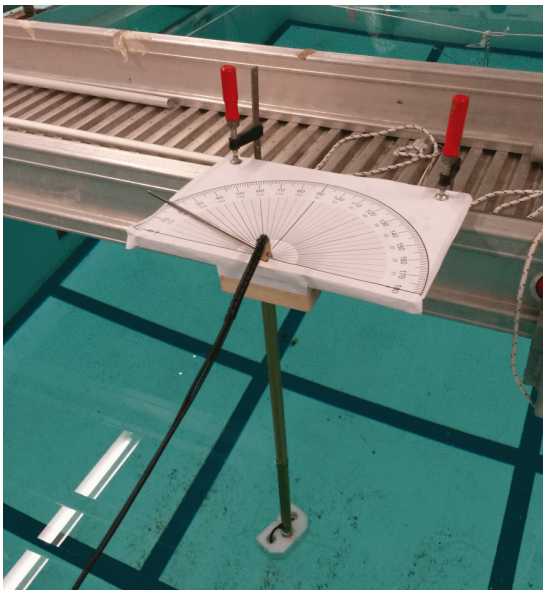

Figure 5.2: The structure used for measuring the angle of the hydrophones.

To accurately measure the angle of the beacon was attached to the hydrophone structure a protractor. With this approach was possible to rotate the axis of the hydrophones with precision relative to the acoustic transmitter. Figure 5.2 shows the structure built for fixing the hydrophones in position and the protractor used for measuring the angle. Figure 5.1 is shown an underwater photograph that displays the beacon in the first plane and the hydrophones behind it.

The experiment consisted of measuring the time difference of arrival for several angles, recording 200 TDOA values for each position. The hydrophones were rotated from $-90°$ to $90°$ in $5°$

steps. It was created an application that runs on the ARM-based processor to configure all the parameters described previously and to store all the values in different files. This program recorded 50 pulses in each angle and saved the 4 TDOA estimates computed by the 4 modules, thus creating one file for each angle with 50 records and 4 delays per record

The time needed to record one file was roughly 60 s, then the program stopped until the hydrophones were rotated to the next angle. When the angle was changed to the next position the application started recording again repeating the process. The output of the experiment was 37 files corresponding to the angles between $-90°$ and $90°$, which adds up to 7400 TDOA estimates.

The files were analyzed using the Matlab software, and it was plotted all the estimates in function of the angle recorded. In figure 5.3 is shown all the delays measured, using a different marker for each TDOA calculator. The black line is the expected theoretical function calculated in section 3.2.

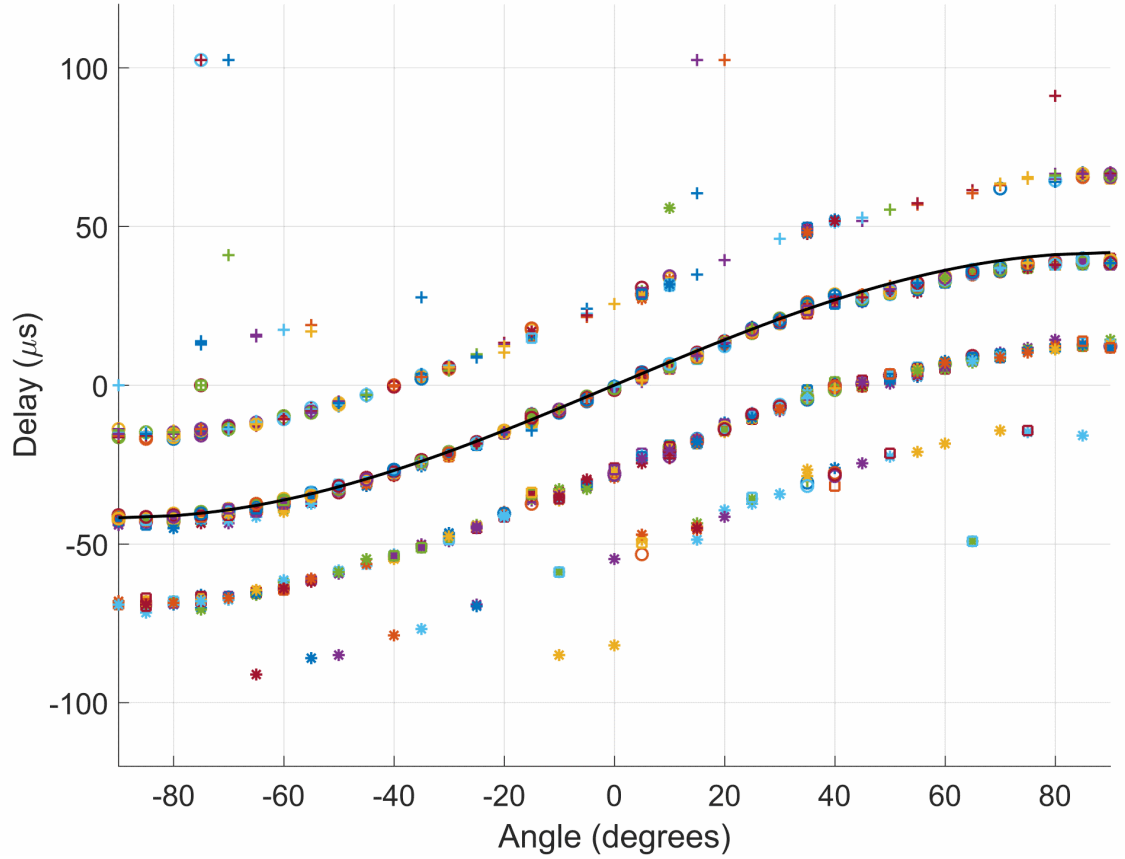

Figure 5.3: The result of the TDOA measurements.

The plot of the estimates shows that most of the points follow one of three lines. The line in the middle is the correct one, the other two are one period above and below the right function. To further analyze these lines was counted the number of points that follow a specific line, the result is shown in figure 5.4.

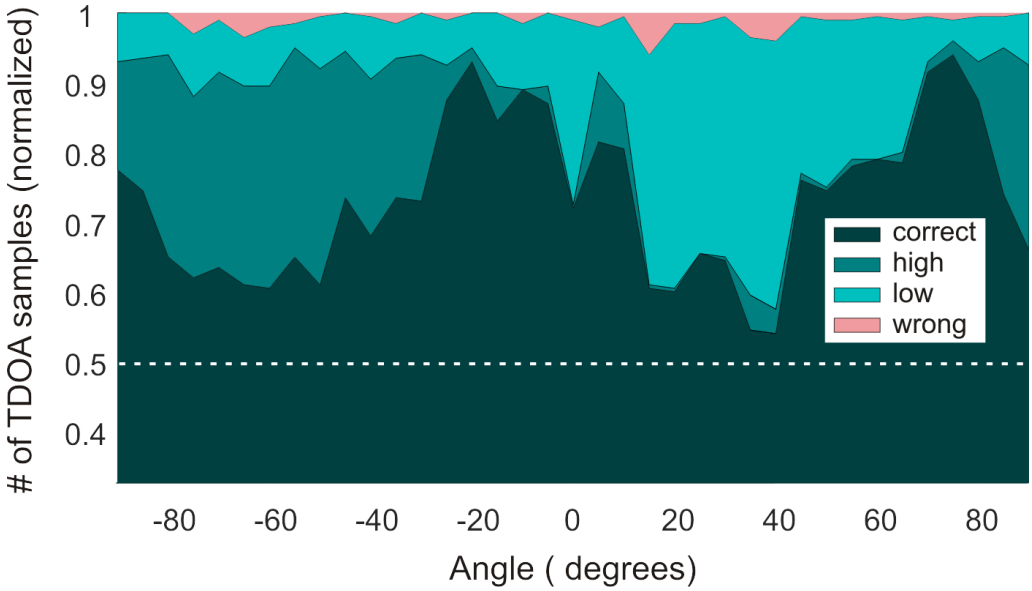

Figure 5.4: Number of estimates that follow specific line.

This figure shows that for all the angles registered, more than 50% of all the estimates are on the theoretical line, and less than 10% do not follow any of the three lines (wrong values). This analysis allows us to conclude that is possible to correct the shifted values by adding or subtracting one period, thus merging the values in the theoretical line.

5.2.1 TDOA Post-processing

As referred in section 4.4, the post-processing analysis of the TDOA estimates was enhanced with the experimental results. It was concluded that for having a good estimate of the angle was needed to compensate the TDOA estimates that are 1 period off. To achieve this in real-time we developed a moving TDOA window with the latest 16 delays that correspond to 4 pulses. Assuming that there are more values in the correct function than in the other two, the values were filtered to have a proper estimate of the delay in the right line. This value its rough estimate of the delay because enters with a lot of different pulses, so it is just used for compensating the latest 4 delays.

The processing of the delay is done in two phases. The first one is the explained above, that consist of getting a rough estimate of the delay but in the correct function. The second stage is an analysis of just the last pulse received, so the latest 4 TDOA estimates. Based on the rough estimate, the four delays are rectified by adding or subtracting a period to match the correct line, after that, are removed any outlier that can be a time-out value or a delay to different from the others. The remaining values are then averaged, and if all the values are discarded is used the last valid estimate.

5.2.2 Different Beacon

To further test the robustness of the implementation and the developed algorithm, we decided to experiment the tracking of a different underwater commercial acoustic beacon. The transmitter used as similar characteristics to the one described in section 4.1.1, but as a pulse frequency of 76 kHz and an acoustic pattern of 4-4-6-5. As this frequency is more than the double of the previous beacon, the resolution measured in samples of the wavelength reduced to less than half of the earlier one, so it was decided to increase the sampling frequency to the double.

Using the decimator factor of 32 instead of 64, the input sample rate of the DSP module changes to almost 4 MHz. All of the modules stay unchanged with this modification except the high pass filter, which duplicates the cut-off frequency resulting in 68 kHz.

The configurable parameters were changed to accommodate these corrections. The following table summarizes all these parameters.

Parameter	**Value**
Decimation factor	32
Threshold-1	85.6%
Threshold-2	93.4%
Number of zeros	12
Maximum delay	51.2 µs
Inactivity time	200 ms
Amplitude time	10 s

Table 5.2: Parameters configuration for experimental tests with a different beacon.

In addition to changing the decimation factor, the zero periods thresholds were altered to the closest integer values in samples to resemble the proportional value of the last experiment. The time period in which the gain module analyzes the maximum amplitude of the signal was changed to catch the at least one pulse of the new beacon's pattern.

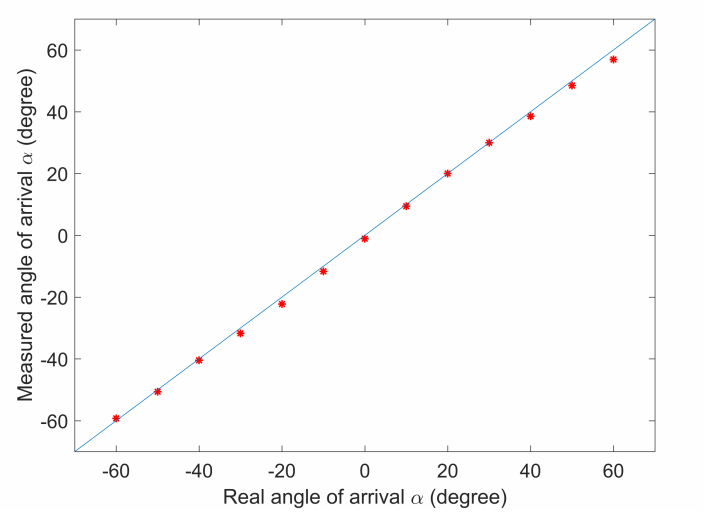

Figure 5.5: The angles measured in comparison with the real ones.

The experiment was done in the test tank with the same configurations described in section 5.2. With a protractor to measure the real angle it was done a sweep from -60° to 60° in 10° steps. In each position it was recorded 20 direction estimates, one for each pulse, then it was averaged to obtain one angle measure. The plot in figure 5.5 shows the result angle for each position in comparison to the real angle. The maximum absolute deviation was 3.1° with a mean error of 1.1°.

This experiment demonstrates the versatility of the system, using a different transmitted signal and sampling frequency without changing the implementation. All the configurations can be modified in real-time allowing the system to track a specific transmitter.

5.3 Field Tests

The laboratory experiments produce good results for the TDOA estimates, therefore, after having a solid delay estimate is straightforward to determine the angle of arrival, is just applying the polynomial functions calculated in section 4.4.

The next logic step was to track the position of the acoustic beacon by measuring the angle of arrival in different positions. The premise was that an autonomous surface vehicle capable of better navigation performance than a long endurance AUV, in terms of speed and maneuverability, can be programmed to sail in a convenient route around an uncertain position of an AUV for improving the estimation of its location.

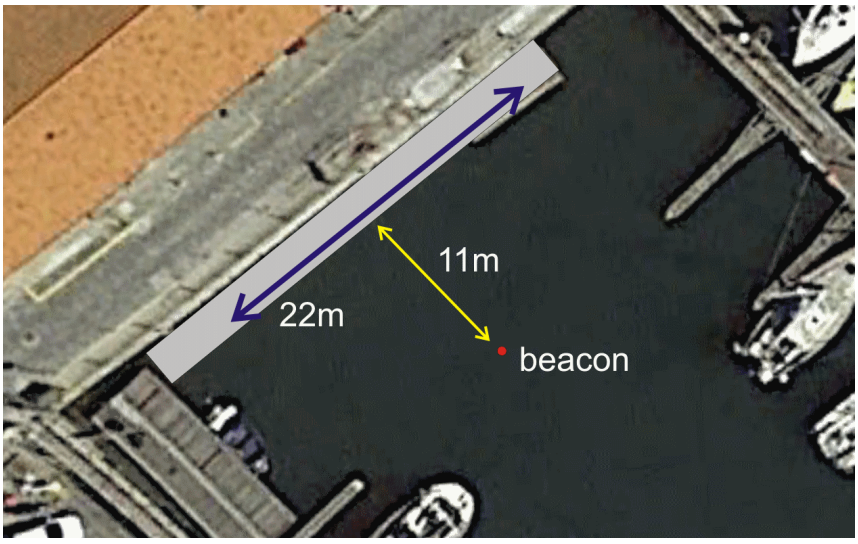

Figure 5.6: The field experiments in the marina of Leixões.

Assuming that the underwater vehicle is a lot slower than the surface vessel, a valid approximation can be that the transmitter is stationary, and the hydrophones are moving. This approach makes the tracking experiment easy to implement.

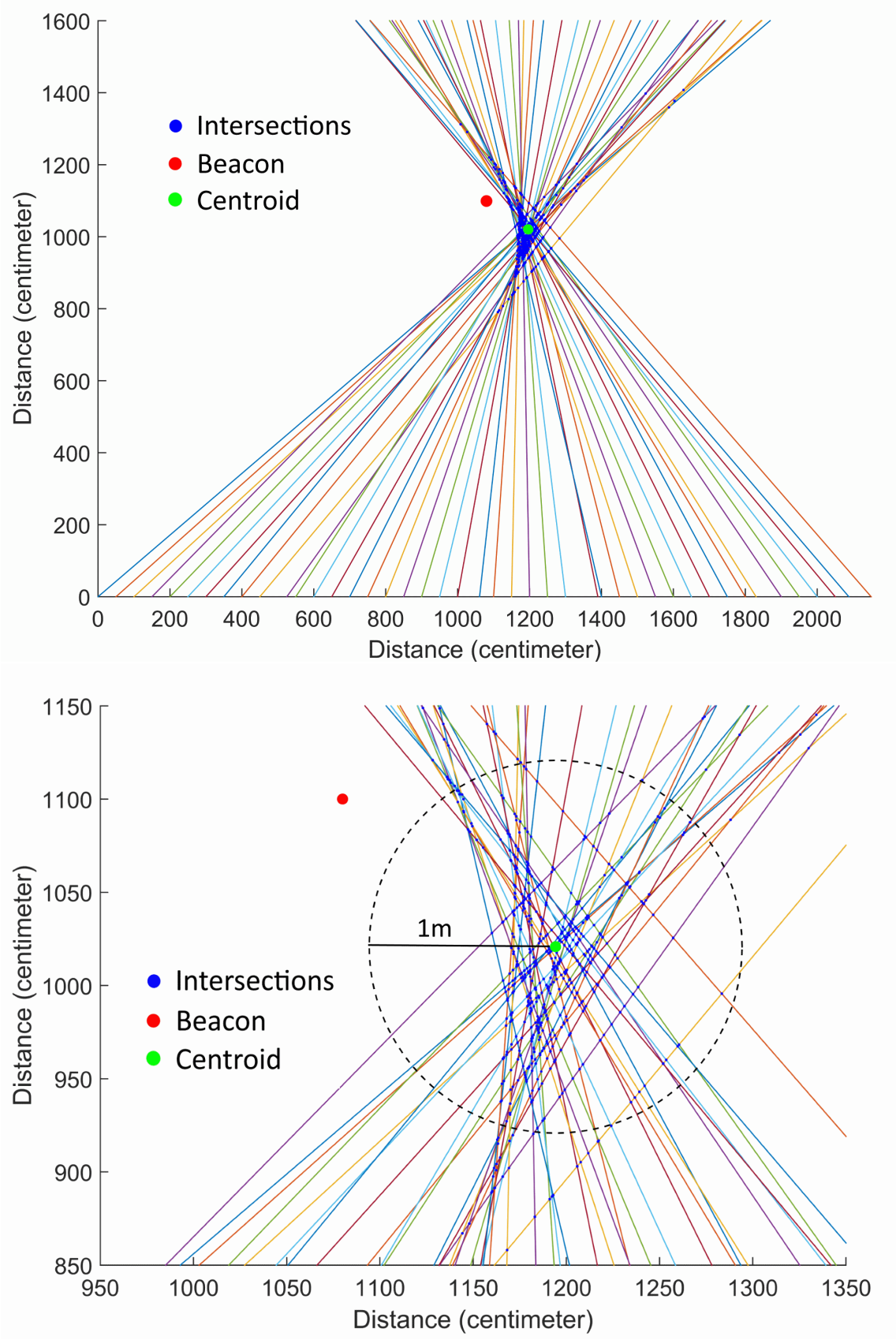

Figure 5.7: Two dimensions plot to track the underwater beacon (top). Close-up on the intersection centroid (bottom).

To approximate the experiment to a realistic scenario was decided to track the beacon in the Leixões port, for having an ample space to move the hydrophones and noise conditions more appropriate to the ocean circumstances. Figure 5.6 shows the scenario of operations in the marina.

The experiment was done with the beacon submerged at 1.5 m deep, 13 m away from any obstacle. The hydrophones were moved 22 m in a straight line along a floating pontoon maintaining a constant direction, where the closest point to the beacon was 11 m, with a constant depth of 1 m.

An application was made to record 20 directions of arrival per positions, as before in each location a new file was created with the 20 estimates. The recording was made in steps of 50 cm, some of the positions were altered by a few centimeters because of obstacles in the floating structure.

The angles recorded was the result of the conversion of individual pulses into TDOA estimates, using the real-time post analysis discussed in section 5.2.1. The files were studied in Matlab to extract the relevant information, in each position was made the average of the angles and plotted a line with the respective direction, as the plot on top of figure 5.7 shows.

The bottom plot of figure 5.7 is a close-up on the intersection area, where the blue dots are the intersection of the lines; these were calculated by intersecting all the lines that start at a distance greater than 3 m, adding up to a total of 742 points. This was opted to avoid remote intersections because the small variations in position produce a minute change in the angle, which can cause the lines being almost parallel and intersect really far from the expected. The green dot is the centroid of all the intersection providing the estimated position of the acoustic transmitter. The red point is the real position of the beacon that has an error associated because was suspended on a rope that inevitably oscillated with the small waves made by moving boats.

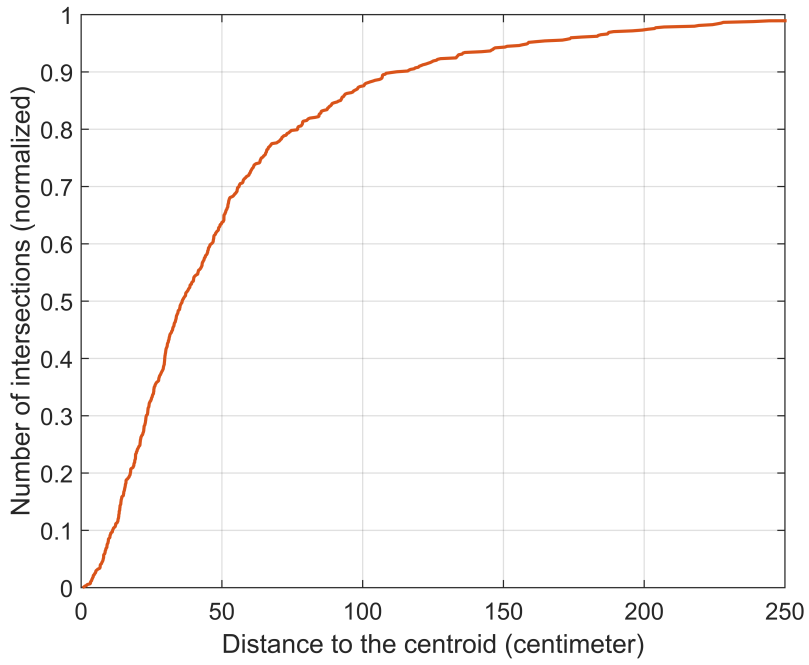

Figure 5.8: Distribution of the intersections relative to the centroid.

As referred before, the goal was to have a relaxed tracking system that allows a surface vehicle to follow the underwater vessel in long missions, so the high precision in the location is not a key element. The centroid of all the intersection is at 1.39 m from the real beacon position, which is not a bad estimate.

The bottom plot of figure 5.7 shows that the intersections are not very dispersed from the center. The black dashed circle as a radius of 1 m and is centered in the centroid, 87.5% of all the intersection are contained in this circle. In figure 5.8 is shown the number of the intersection due to the distance to the centroid, which reveals the high density of points close to the centroid.

After this analysis, the accuracy in the position tracking can be enhanced with proper calibration of the system, because the focus of the intersections are clearly away from the real location of the transmitter. This can be induced by small variations in the hydrophones axis angle, a difference in the spacing of the hydrophones or tilt.

The range of the system was tested too, in the marina scenario, the maximum distance which the measurements were stable was about 20 m from the transmitter, farther than that, the analog signal amplifier reached the maximum gain. The noise was so amplified that signal was almost unrecognizable, and the system did not work properly.

Summary

In this chapter it was presented the two principal experiments done in this work. Firstly, it is explained the hardware parameters used in the configurable modules. Afterwards, it is presented the first practical experiment for the validation of the TDOA estimates with the correspondent angle of arrival, and the conclusions are added to enhance the post-processing phase. In the laboratory experiments was tested a different beacon to demonstrate the versatility of the system. Lastly, was made the tracking experiment in the marina, with the real-time estimation of the angle of arrival, and the posterior analysis of the tracking results, culminating in the estimation of the beacon's location.

Chapter 6

Conclusions

The approach in this thesis was to develop a low-cost and low-power underwater positioning system that could be employed in a long-endurance surface vehicle. To reduce computational effort and the infrastructure complexity was created an alternative method to determine the TDOA.

In chapter 3 it was analyzed the signals recorded by the hydrophones, verifying that the underwater environment introduces several distortions in amplitude and phase of the sound waves, due to reflections and the variation of the sound propagation speed with temperature, pressure and salinity. Particularly in confined spaces, the high level of reverberation makes the amplitude of the signals captured by the hydrophones very dissimilar, and because of this, the use of the cross-correlation method is not effective to identify the time difference of arrival.

In this work, we propose an alternative method to calculate the TDOA consisting in the detection of the beginning of the signals by discovering a series of zero crossing samples looking alike in each received signal, and then calculating the time difference between them. The realization of this method is presented in chapter 3, as the process to determine the direction of arrival of the acoustic wave by the TDOA estimate. It was concluded that in a two-dimensional spatial configuration the trilateration and multilateration method have similar results, but with different theoretical functions. As both approaches are computationally heavy for real-time calculations, in chapter 4 it was decided to fit the trilateration function with low order polynomial functions, to ease the implementation in the software processing unit.

In chapter 4 is presented the successful hardware implementation of the zero crossing algorithm in the RedPitaya single board computer. The hardware equipment utilized is presented, like the commercial underwater acoustic beacon used as the transmitter and the analog front-end board, where the two hydrophones are connected. The digital integration is divided into several modules, which are described individually. In this section is described the implementation of the high-pass filter, the amplitude determination module, and the TDOA calculator.

The application running on the ARM processor is also defined in chapter 4, this section contains the automatic gain controller of the analog amplifiers, the clarification of all the configurable parameters, and the DOA determination.

The chapter 5 contains the results and conclusions of the practical experiments. Firstly, was

determined the hardware parameters used to configure modules. Afterward, in the test tank of water was tested the prototype by measuring the time difference of arrival for several angles, then was analyzed the results, allowing the enhancement of software post-processing filters.

In the laboratory was also done another experiment to demonstrate the versatility of the system, using a different transmitted signal and sampling frequency without changing the implementation. All the configurations can be modified to track a specific transmitter allowing the system to change the in real-time the beacon to track.

Lastly, in the marina environment was recorded real-time estimations of the angle of arrival in different positions along a straight line, wherein after an analysis of the directions was successfully located the fixed transmitter.

6.1 Future Work

Several improvements can be added to this work; these can correct some of the problems encountered and enhance the prototype characteristics.

- Employing high-quality hydrophones with differential output to decrease the noise and increase the range of the system.
- Apply to the structure an inertial measurement unit to compensate inclinations or changes in direction.
- Testing with different acoustic transmitters with various frequencies and patterns to validate the prototype.
- Employing more than two hydrophones to achieve a better angle precision and three-dimensional tracking.
- Applying the system to an autonomous surface vehicle and establishing convenient navigation patterns to improve the estimation of the actual position of the transmitter.

References

Sonotronics Inc. (2016). Equipment marking transmitters. Available from: http://www.sonotronics.com/?page_id=119.

Alcocer, A., Oliveira, P., and Pascoal, A. (2006). Underwater acoustic positioning systems based on buoys with gps. In *Proceedings of the Eighth European Conference on Underwater Acoustics*, volume 8, pages 1–8.

Alves, J. C. and Cruz, N. A. (2008). Fast-an autonomous sailing platform for oceanographic missions. In *OCEANS 2008*, pages 1–7. IEEE.

Chen, J., Benesty, J., and Huang, Y. (2006). Time delay estimation in room acoustic environments: an overview. *EURASIP Journal on applied signal processing*, 2006:170–170.

Curcio, J., Leonard, J., Vaganay, J., Patrikalakis, A., Bahr, A., Battle, D., Schmidt, H., and Grund, M. (2005). Experiments in moving baseline navigation using autonomous surface craft. In *OCEANS, 2005. Proceedings of MTS/IEEE*, pages 730–735. IEEE.

Dalskov, D. and Olesen, S. K. (2014). Locating acoustic sources with multilateration. Master's thesis.

Desert Star Systems (2015). Pilot system (accessed jan 2016. Available from: http://desertstar.com/product/pilot-system/.

Eustic, R. M., Whitcomb, L. L., Singh, H., and Grund, M. (2007). Experimental results in synchronous-clock one-way-travel-time acoustic navigation for autonomous underwater vehicles. In *Robotics and Automation, 2007 IEEE International Conference on*, pages 4257–4264. IEEE.

Ferreira, B. M., Matos, A. C., Cruz, N. A., and Almeida, R. M. (2012). Towards cooperative localization of an acoustic pinger. In *Oceans, 2012*, pages 1–5. IEEE.

Folk, A., Armstrong, B., Wolbrecht, E., Grip, H. F., Anderson, M., and Edwards, D. (2010). Autonomous underwater vehicle navigation using moving baseline on a target ship. In *OCEANS 2010*, pages 1–7. IEEE.

Klungmontri, C., Nilkhamhang, I., Covanich, W., and Isshiki, T. (2015). Underwater positioning systems for underwater robots using trilateration algorithm. In *Information and Communication Technology for Embedded Systems (IC-ICTES), 2015 6th International Conference of*, pages 1–5. IEEE.

Kongsberg Maritime (2016). Hipap xx2 - acoustic underwater positioning and navigation systems. Available from: https://www.km.kongsberg.com/ks/web/nokbg0240.nsf/AllWeb/9DC12B00C48A0B63C1257F0900319BCF.

Leonard, J. J., Bennett, A. A., Smith, C. M., and Feder, H. (1998). Autonomous underwater vehicle navigation. In *IEEE ICRA Workshop on Navigation of Outdoor Autonomous Vehicles, Leuven, Belgium, May*. Citeseer.

LinkQuest Inc. (2016). Lbl applications. Available from: http://www.link-quest.com/html/lbl_applications.htm.

Liu, S., Zhang, C., and Huang, Y. (2012). Research on acoustic source localization using time difference of arrival measurements. In *Measurement, Information and Control (MIC), 2012 International Conference on*, volume 1, pages 220–224. IEEE.

Papadopoulos, G., Fallon, M. F., Leonard, J. J., and Patrikalakis, N. M. (2010). Cooperative localization of marine vehicles using nonlinear state estimation. In *Intelligent Robots and Systems (IROS), 2010 IEEE/RSJ International Conference on*, pages 4874–4879. IEEE.

Paull, L., Saeedi, S., Seto, M., and Li, H. (2014). Auv navigation and localization: A review. *Oceanic Engineering, IEEE Journal of*, 39(1):131–149.

Rowan, E. (2008). Lbl underwater positioning. *Hydro International*, 12(1).

Rui, G. and Chitre, M. (2010). Cooperative positioning using range-only measurements between two auvs. In *OCEANS 2010 IEEE-Sydney*, pages 1–6. IEEE.

Safran Electronics Defense (2014). Navigation systems. Available from: http://www.sagem.com/naval-solutions/submarines/navigation-systems.

Schau, H. and Robinson, A. (1987). Passive source localization employing intersecting spherical surfaces from time-of-arrival differences. *Acoustics, Speech and Signal Processing, IEEE Transactions on*, 35(8):1223–1225.

Sonardyne International Ltd. (2016). Usbl all systems. Available from: http://www.sonardyne.com/products/positioning/usbl-all-systems.html.

Tan, H.-P., Diamant, R., Seah, W. K., and Waldmeyer, M. (2011). A survey of techniques and challenges in underwater localization. *Ocean Engineering*, 38(14):1663–1676.

Teledyne Webb Research Corporation (2016). Electric glider @ONLINE. Available from: http://www.webbresearch.com/electricglider.aspx.

Thomas, H. C. (1998). Gib buoys: an interface between space and depths of the oceans. In *Autonomous Underwater Vehicles, 1998. AUV'98. Proceedings of the 1998 Workshop on*, pages 181–184. IEEE.